Geomechanics and Engineering, *Vol. 35, No. 4 (2023) 333-366*
https://doi.org/10.12989/gae.2023.35.4.333

A review of experimental and numerical studies on crack growth behaviour in rocks with pre-existing flaws

G. Sivakumar*[1] and V.B. Maji[2a]

[1]*Department of Civil Engineering, Indian Institute of Technology Jammu, Jammu, Jammu and Kashmir 181221, India*
[2]*Department of Civil Engineering, Indian Institute of Technology Madras, Chennai, Tamil Nadu 600036, India*

(*Received May 7, 2022, Revised July 10, 2023, Accepted October 12, 2023*)

Abstract. Rock as a mass generally exhibits discontinuities, commonly witnessed in rock slopes and underground structures like tunnels, rock pillars etc. When these discontinuities experiences loading, a new crack emerges from them which later propagates to a macro scale level of failure. The failure pattern is often influenced by the nature of discontinuity, geometry and loading conditions. The study of crack growth in rocks, namely its initiation and propagation, plays an important role in defining the true strength of rock and corresponding failure patterns. Many researchers have considered the length of the discontinuity to be fully persistent on rock or rock-like specimens by both experimental and numerical methods. However, only during recent decades, there has been a substantial growth in research interest with non-persistent discontinuities where the crack growth and its propagation phenomenon were found to be much more complex than persistent ones. The non-persistence fractures surface is generally considered to be open and closed. Compared to open flaws, there is a difference in crack growth behaviour in closed or narrow flaws due to the effect of surface closure between them. The present paper reviews the literature that has contributed towards studying the crack growth behaviour and its failure characteristics on both open and narrow flaws subjected to uniaxial and biaxial compression loading conditions.

Keywords: biaxial compression; non-persistent discontinuity; pre-existing flaw; uniaxial compression

1. Introduction

The failure mode in rock differs under different stress conditions and can provide valuable information about rock strength and deformational characteristics for safe and economical design. It mainly depends on the crystalline aggregate's strength, anisotropy, brittleness, and grain size. In the case of intact rock, failure by axial fracturing generally precedes faulting and characterizes failure initiation at 50-95 per cent of the compressive strength (Wawersik and Fairhurst 1970, Hoek and Martin 2014). The experiments suggest that the compressive strength of rock is governed by the formation of the macroscopic fault and by local fracturing predominantly parallel to the direction of the loading. Szwedzicki (2007) stated that understanding the effect of the mode of failure on strength enables a good interpretation of the results of the UCS tests (Fig. 1(a)).

When the rock samples are subjected to triaxial stresses, their peak strength increases with the increase in confining pressure due to the interlocking of fractures (Goodman 1989). With a moderate amount of confining pressure, longitudinal fracturing is suppressed and failure occurs along a clearly defined plane of fracture (Fig. 1(b)). The rock behaves like ductile material at a very high confining pressure (Jaeger *et al.* 2007). Also, the change in confining pressures alters the fracturing phenomenon from tensile fracturing to macro-scale shear failure. This behaviour is due to an increase in micro-cracks density and its ultimate coalescence leading to strain localization of the sample (Hoek and Martin 2014). However, discontinuities are usually encountered in the field in the rock mass. They commonly originate from geological processes such as folding/fault movement, tectonic forces, volcanic eruptions etc. Also, in engineering operations such as mining,

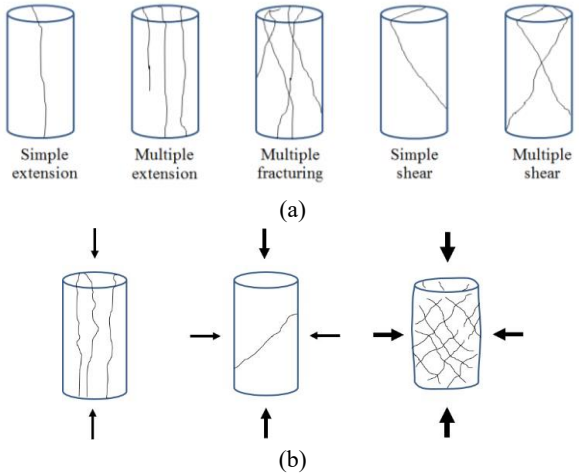

Fig. 1 (a) Common failure modes of rock samples under uniaxial compression (after Szwedzicki 2007) and (b) under effect of confining pressure (adopted from Jaeger *et al*. 2007)

*Corresponding author, Assistant Professor
E-mail: sivakumar.g516@gmail.com
[a]Professor

ISSN: 2005-307X (Print), 2092-6219 (Online)

(a)

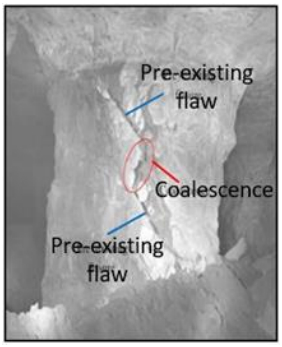

(b)

Fig. 2 (a) Landslide in Kinnaur district (Himachal Pradesh, India) due to presence of a discontinuity in rock mass and (b) Coalescence failure observed in pillar fissure located at underground excavation in US (after Esterhuizen *et al.* 2011)

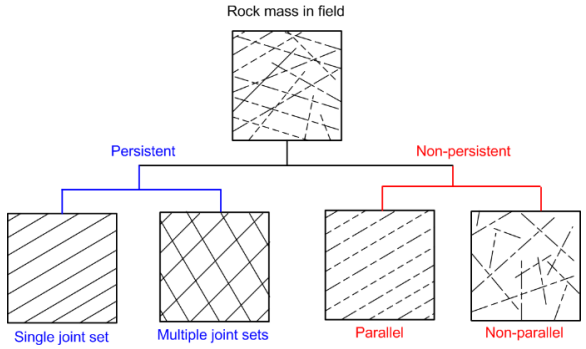

Fig. 3 Possible formation of discontinuities sets that are usually encountered in a rock mass (adopted from ISRM 1978)

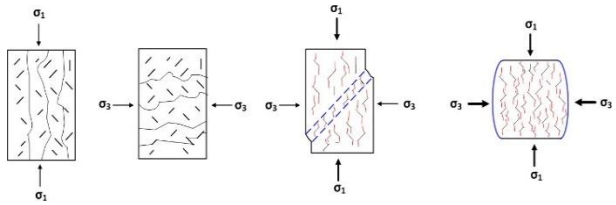

Fig. 4 Failure of rock due to presence of discontinuity subjected to different compressive stress states

tunnelling, caverns, etc., a new fracture may develop around the excavated portion. These discontinuities are usually planar and have relatively smooth surfaces and generally less relative displacement is observed. When the surface undergoes a movement from this plane of weakness, it causes the fractures to open. The rock with pre-existing fractures fails by coalescence formation between several micro-cracks and leads to macroscopic failure (Fig. 2).

Joints/fractures are often visible in the field as a group and occur as a set which can be parallel or non-parallel. The length or extent of the fractures is termed persistence, and their joint sets generally affect the stability of the rock mass. The fracture in the rock mass as a group can be persistent (cross the other joints), sub-persistent (half persistent and another non-persistent) or non-persistent sets as shown in Fig. 3. The fracture sets may exhibit orientation, where they can be parallel or non-parallel to each other. In the case of fully persistent fractures, which are continuous throughout the rock domain, the failure mechanism is based on the translational failure along the fracture plane surface.

According to An *et al.* (2014), in the field cases of massive rock slopes and deeply excavated slopes, persistent fractures are very unlikely. The slope failure observed in the field is undergone to have the complex interaction between non-continuous existing fractures and brittle propagation through intact rock bridges. It is understood that a rock mass's strength and deformation behaviour largely depend on the intact portion and the joint characteristics. In turn, joints or discontinuities in the rock mass depend on the small cracks or flaws, their growth under different loading environments, and their interaction.

Studies on the mechanical behaviour of fully persistent joints were carried out and investigated by many researchers (Amadei and Goodman 1981, Jade and Sitharam 2003, Trivedi 2013, Wang and Huang 2009), whereas the studies on non-persistent fracture are limited.

The mechanism of the non-persistent fractures, when subjected to external loading on rock, leads to the development of a new crack and its propagation (Shemirani *et al.* 2017). Non-persistent fractures are often seen in ceramics, rocks and minerals, where fine microcracks are present equal to the grain size caused by elastic or thermal stress during loading (Ashby and Hallam 1986). The cracks start propagating when they nearly reach the axial compressive stress state and are mostly extended towards the loading direction. The material's failure behaviour was influenced by the confining pressure where the propagated cracks attain failure at the maximum compressive stress.

The interaction pattern between the cracks can lead to macro shear failure to ductile failure with an increase in confinement (Fig. 4).

The studies on non-persistent fracture are initially performed by the experimental method based on rock or rock-like materials subjected to compressive loads (Bobet and Einstein 1998 a,b, Sagong and Bobet 2002, Wong and Einstein 2009a, b, c, Park and Bobet 2009, 2010). The flawed surface is considered open and the surface is assumed to remain open throughout the loading. In the case of narrow flaw configuration, the initially open surface upon loading gets closed and eventually experiences a frictional effect in between the surface. Due to the closure effect, the crack stresses were observed to initiate at higher stress levels and different crack propagation trajectories

Table 1 Types of the material adopted in experiments to study the failure behaviour of non-persistent fractures

Material adopted	Flaw type	Geometry	References
Uniaxial compression			
Plaster of Paris	Open	Single flaw	Lajtai (1974)
Glass	Open	Single flaw	Ingraffea and Heuze (1980)
	Closed	Single flaw	Hoek and Bieniawski (1965)
Poly Methyl Meth Acrylate (PMMA)	Open	Single flaw	Ingraffea and Heuze (1980), Petit and Barquins (1998), Lee and Jeon (2011)
		Single flaw and double flaws (non-parallel)	
Plastic polymer	Open	Single flaw	Ingraffea and Heuze (1980)
Limestone	Open	Single flaw	Ingraffea and Heuze (1980)
Marble	Open	Single flaw	Huang *et al.* (1990), Chen *et al.* (1995), Wong *et al.* (2006), Wong and Einstein (2009a)
Gabbro	Open	Single flaw	Wong *et al.* (2006)
Sandstone	Open	Single flaw	Wong *et al.* (2006), Yang and Jing (2011), Miao *et al.* 2022
		Single and combined flaws	Yang (2015)
		Filled flaw	Miao *et al.* 2022
	Closed	Double flaw (parallel)	Wong and Chau (1998)
Granite	Open	Single flaw	Wong *et al.* (2006), Lee and Jeon (2011)
Gypsum	Open	Single flaw	Wong and Einstein (2009a)
		Double flaw (parallel)	Bobet and Einstein (1998a), Wong and Einstein (2009b,c), Reyes and Einstein (1991)
		Double flaw (non-parallel)	Afolagboye *et al.* (2018)
		Three and Sixteen flaws (parallel)	Sagong and Bobet (2002)
	Closed	Double flaw (parallel)	Bobet and Einstein (1998), Shen *et al.* (1995)
		Single flaw and double flaws (non-parallel)	Sivakumar and Maji (2018, 2021)
Concrete	Open	Three flaws (parallel)	Sarfarazi *et al.* (2021, 2022)
		Five flaws (parallel and intersecting)	Amini *et al.* (2021)
Cement Mortar	Open	Single flaw	Jin *et al.* (2017)
	Closed	Double flaw (parallel)	Zhao *et al.* (2016)
Diastone	Open	Single flaw and double flaws (non-parallel)	Lee and Jeon (2011)
Cement-sand mixture	Open	Double flaw (parallel)	Mughieda and Karasneh (2006)
Biaxial compression			
Poly Methyl Meth Acrylate (PMMA)	Open	Single flaw	Petit and Barquins (1998)
Gypsum	Open and Closed	Double flaw (parallel)	Bobet and Einstein (1998)

compared to open flaw conditions (Hoek and Bieniawski 1965, Park and Bobet 2009, 2010, Vásárhelyi and Bobet 2000). Researchers have also further extended the study into numerical analysis to investigate the crack growth behaviour in the field under different loading conditions. In both studies, understanding the philosophy of failure modes in rock corresponding to crack initiation and propagation would be vital in rock engineering applications. The aim of present study is to give a comprehensive review of the crack growth behaviour with respect to crack initiation, propagation and coalescence behaviour on rock or rock-like material considering both open and narrow flaws. This study mainly focuses on the crack growth behaviour based on flaw geometry, loading conditions and failure characteristics from experimental and numerical findings.

2. Experimental study

The laboratory studies are discussed first on single flaw configuration to observe the crack types based on initiation nature. The initiated cracks get propagated with the increase in loading; however, their cracking trajectories were influenced by flaw configuration like surface closure, flaw angle and nature of loading. Subsequently, the studies are extended into double and multiple flaws to understand the

coalescence effect between the flaws. The flawed geometrical arrangements and loading conditions affect the coalescence behaviour and nature. Table 1, summarizes the adopted literature based on experimental studies that is been discussed in the following section.

2.1 Open flaw

The sequence of the crack growth of a single open flaw under uniaxial compression was first summarized by Lajtai (1974). The study was conducted on a Plaster of Paris specimen with different flaw orientations to the loading directions. The first/primary crack observed from the flaw tip was tensile, which was observed to propagate in a curvilinear path and later aligned parallel to the direction of loading. Further, high compressive stresses were observed at the flaw tip region, where a shear zone formed around the flaw tip. When the loading is further increased, initially, a secondary crack of shear nature was observed to propagate in a direction normal to the loading (Fig. 5). Later at the same tip, another crack of shear nature inclined in the shear zone region was observed, resulting in complete material failure. Based on the experimental study on different materials, namely, glass, Poly Methyl Meth Acrylate (PMMA), plastic polymer and limestone, Ingraffea and Heuze (1980) classified the fracturing behaviour for primary and secondary cracks under uniaxial compression. The primary cracks were observed to initiate generally at the point where high tensile stress is observed in the material. The initiated crack upon loading propagates towards the top and bottom boundary of the specimen. In the case of secondary cracks, they originate from the area where compressive stress concentration was seen and appears only in rock. It was noticed that the secondary cracks usually propagate in an unstable manner compared to tensile crack growth.

However, the developments of crack types are quite different in rock material for marble, as observed by Huang *et al.* (1990). An additional fully developed tensile crack

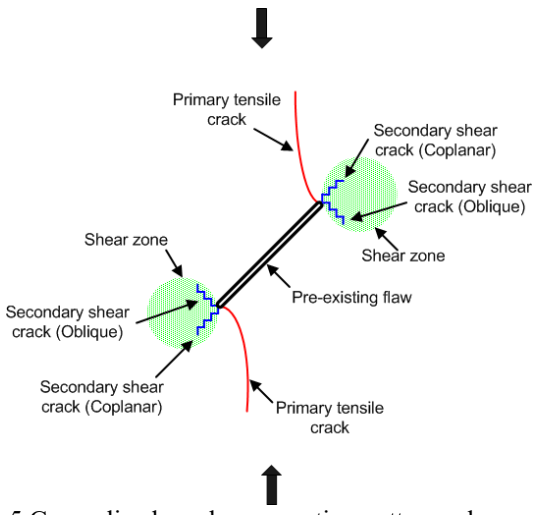

Fig. 5 Generalized crack propagation patterns observed in specimen with pre-existing flaw under uniaxial compression

and a backward tensile crack were observed, opposite to the location of the conventional wing crack along with the existing tensile crack (Fig. 6). Further, the observed rupture of the material was governed by a fully formed shear belt region when the flaw angle is less than 45° to the loading direction. With an increase in flaw angle, the rupture of the material is governed by a backward tensile crack which causes the axial splitting of the specimen assisted with a shear belt. It was further verified by Chen *et al.* (1995) from experimental study on marble specimens where the presence of the initiated cracks did not consistently influence the failure of the material. In their experiments, the belt region was observed as an 'X' shaped band observed around the flaw region along with the formation of a secondary crack, which causes the material to attain its failure (Fig. 7). The study correlates the primary crack as tensile nature similar observation by Ingraffea and Heuze's (1980) study, however the nature of the secondary crack was not appropriately defined. According to them, the secondary cracks were observed in an area where compressive stress present, which is quite different from Ingraffea and Heuze's observations. The backward tensile wing crack was later termed the 'anti-wing' crack by Wong *et al.* (2006) on the Gabbro specimen. Based on their observation of natural rocks like gabbro, marble, sandstone and granite, in most tests, the location of this crack may or may not originate at the flaw tip (Fig. 8). The cracks which were initiated were found to approach towards the flaw tip and link with the flaw surface at the compressive region, and later, a secondary tensile crack appears at the same flaw tip in the tensile region. According to Petit and Barquins (1998), the formation of shear cracks, under uniaxial compression, was initially observed as echelon microcracks from the shear zone in both coplanar and quasi-planar directions to the flaw surface. They observed this behaviour for PMMA material with a single pre-existing flaw subjected to uniaxial and biaxial compression (Fig. 9). When the stress state changes to the biaxial condition, the formation of echelon microcracks was more pronounced in the shear zone and extended in the coplanar direction, causing the material to fail in a shear manner.

In most of the earlier studies, the terms primary cracks, tensile cracks and wing cracks are interchangeably used. Similarly, the terms secondary cracks and shear cracks are interchangeably used.

Later, the nature of different crack types and their systematic behaviour were clearly defined by Wong and Einstein (2009a) with new experimental techniques using a high-speed camera (Fig. 10). The test was performed on prismatic moulded gypsum and Carrara marble specimens with different flaw angles. Based on the observations from the studies, the term primary crack was used to define the crack that is first observed from the flaw tips, not based on the tensile or shear nature of the crack. The crack observed after the primary crack was defined as the secondary crack. From the experiments conducted on marble and gypsum specimens, it was observed that the tensile cracks that appear first with high flaw inclination subsequently led to the specimen failure. A mixed-mode tensile-shear crack was commonly observed for low flaw inclination angles. The

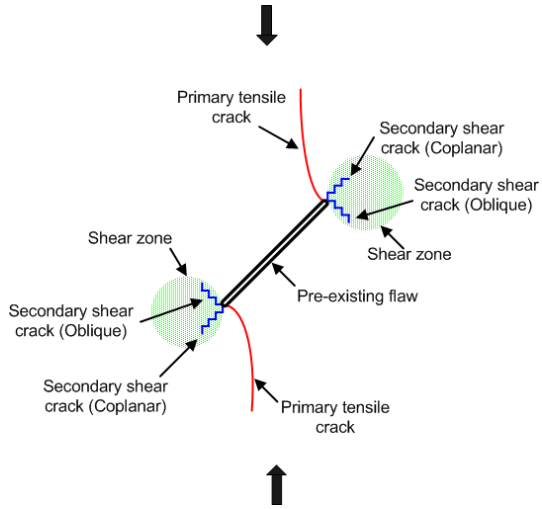

Fig. 6 Formation of shear belt observed along with tensile cracks (adopted from Huang *et al*. 1990)

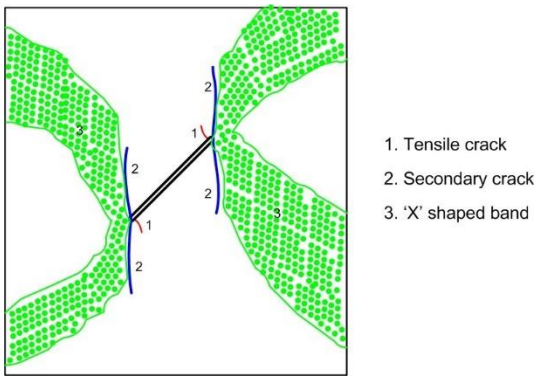

Fig. 7 X-shaped band growth observed in marble specimen containing a single flaw (adopted from Chen *et al.* 1995)

crack initially appears coplanar to the flawed surface and later inclines to form a curvilinear-like wing crack. The presence of shear cracks was commonly observed during the later stage of loading, and they are commonly seen only in marble specimens compared to gypsum material. The propagation of shear cracks was independent of the flaw angle, which inclines and fails at an angle of 55° - 65° to horizontal. It was also mentioned that the usage of the terminologies primary and secondary does not indicate the crack nature but a temporal relationship to classify them. Apart from types of crack growth and their mechanism, the material properties were influenced by the factors such as flaw length and flaw angle based on an investigation by Yang and Jing (2011) on sandstone specimens. Their experimental study on sandstone specimens attempted to understand the material's load and deformation up to failure using photographic monitoring and the Acoustic Emission (AE) technique. The strength of the material was found to decrease with an increase in flaw length. The mechanical properties such as Young's modulus, peak strength, and corresponding axial strain were smaller than intact rock conditions. Unlike intact material, where material fails in axial splitting, flawed specimen failure was observed by localization of deformation in the material. Nine different types of cracks were identified in their study based on flaw angle and crack growth mechanism (Fig. 11). Apart from tensile (TS) and shear crack (SC), other new types of cracks such as lateral crack (LC), far-field crack (FC) and surface spalling (SSC) were identified and classified as per their mechanism. According to their experiments, the tensile crack is often first initiated mostly from the tips of the pre-existing fissure. The shear crack usually occurs for fissures having a longer length and propagates coplanar to the aperture. In contrast, the lateral crack initially initiates along the fissure and later orientates towards a horizontal direction. The far-field cracks usually propagate away from the flaw tip, which may be vertical or horizontal, and surface spalling usually appears after the tensile crack. The strength of the material under different flaw angles was studied by Jin *et al.* (2017) on cement mortar specimens. For low flaw angles (0° - 30°), the failure of the specimen was influenced by tensile crack, and the crack initiation position was found away from the flaw tip (Fig. 12(a)). When the angle increases greater than 45°, the crack mainly develops from the flaw tips and the flaw surface experiences relatively less shear. The specimen's strength was found to increase with an increase in flaw angle in their study (Fig. 12(b)).

Subsequently, researchers studied the effect of coalescence behaviour between the flaws and their corresponding failure pattern by considering double flaw or multiple flaw configurations. The coalescence behaviour in gypsum specimens having two flaws subjected to uniaxial compression was s-tudied by Reyes and Einstein (1991). The flaw geometrical arrangements were kept parallel to each other and the bridge angle, i.e., the angle formed between the inner tips of both the flaw with respect to horizontal is varied, as shown in Fig. 13(a). Based on the bridge angle between the two flaws, the flaw geometries are classified as non-overlapping (< 90°) and overlapping geometries (>90°). Three modes, namely, tensile (T), shear (S) and mixed-mode (M) (tensile and shear both) nature coalescences are observed from their experiments (Fig. 13(b)). The tensile coalescence through the extension of tensile cracks and shear coalescence from shear cracks were observed for overlapping geometry and non-overlapping flaws respectively. The mixed-mode coalescence was observed forming either by the tensile fracturing, shearing, or a combination of both. The behaviour of coalescence under uniaxial and biaxial compression was studied by Bobet and Einstein (1998). The study was performed on gypsum specimens having parallel flaw of non-overlapping geometries. Their experimental studies showed that in uniaxial compression, the coalescence stress and peak stress were observed simultaneously. Whereas, in case of biaxial compression the peak stress is observed after coalescence. Also, the growth of wing cracks was found to decrease with an increase in confinement and at higher confinement, coalescence was formed by shear cracks (Fig. 14). Further, studies by Mughieda and Karasneh (2006) showed that the strength of the specimen was found to be higher for coplanar flaw compared to the stepped flaw configuration.

They performed biaxial compression on a rock-like material (cement-sand mixture) with non-overlapping flaw

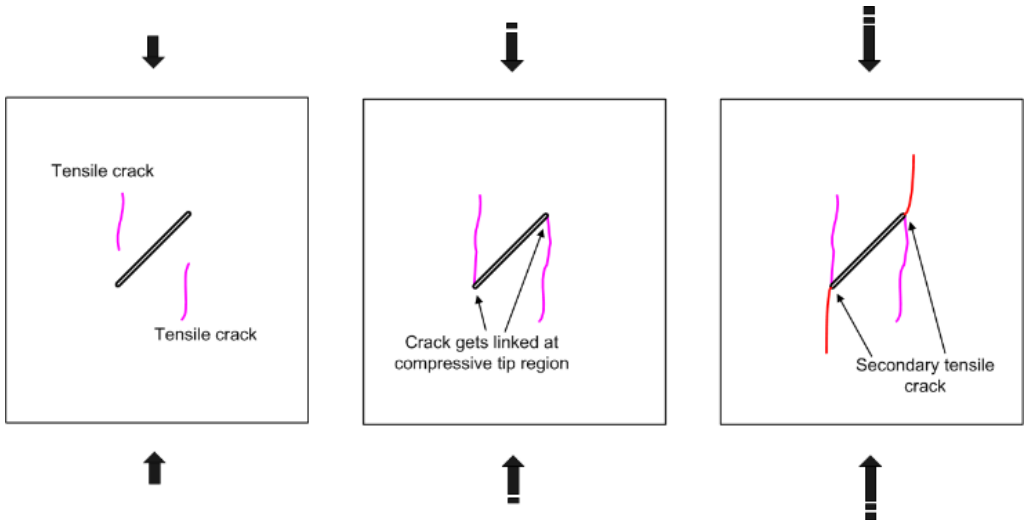

Fig. 8 Sequential formation of anti-wing crack and secondary tensile crack in Gabbro specimen (adopted from Wong *et al.* 2006)

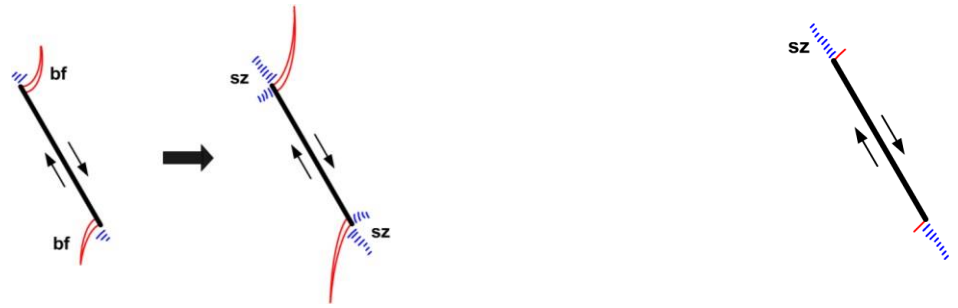

(a) (b)

Fig. 9 Formation of branch fracture (bf) and shear zone (sz) observed in PMMA under (a) uniaxial and (b) biaxial compression (adopted from Petit and Barquins 1998)

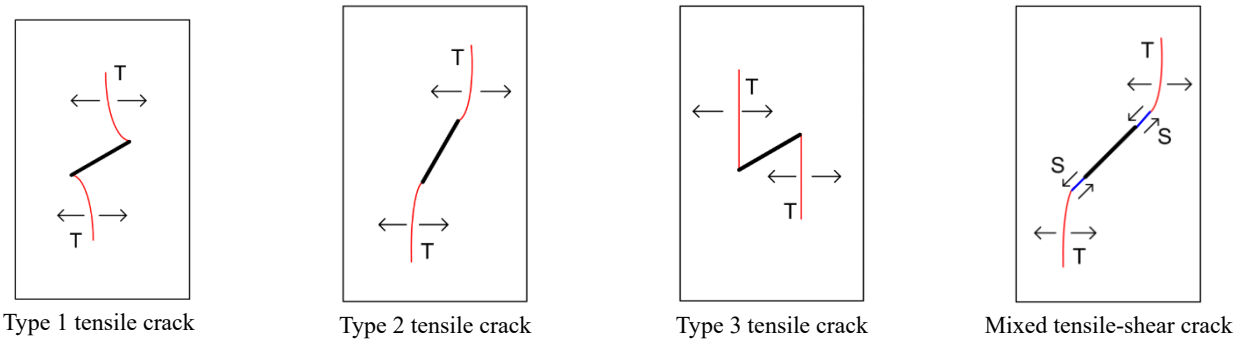

Type 1 tensile crack | Type 2 tensile crack | Type 3 tensile crack | Mixed tensile-shear crack

Type 1 shear crack | Type 2 shear crack | Type 3 shear crack

Fig. 10 Crack types found in a single flaw under uniaxial compression (adopted from Wong and Einstein 2009a)

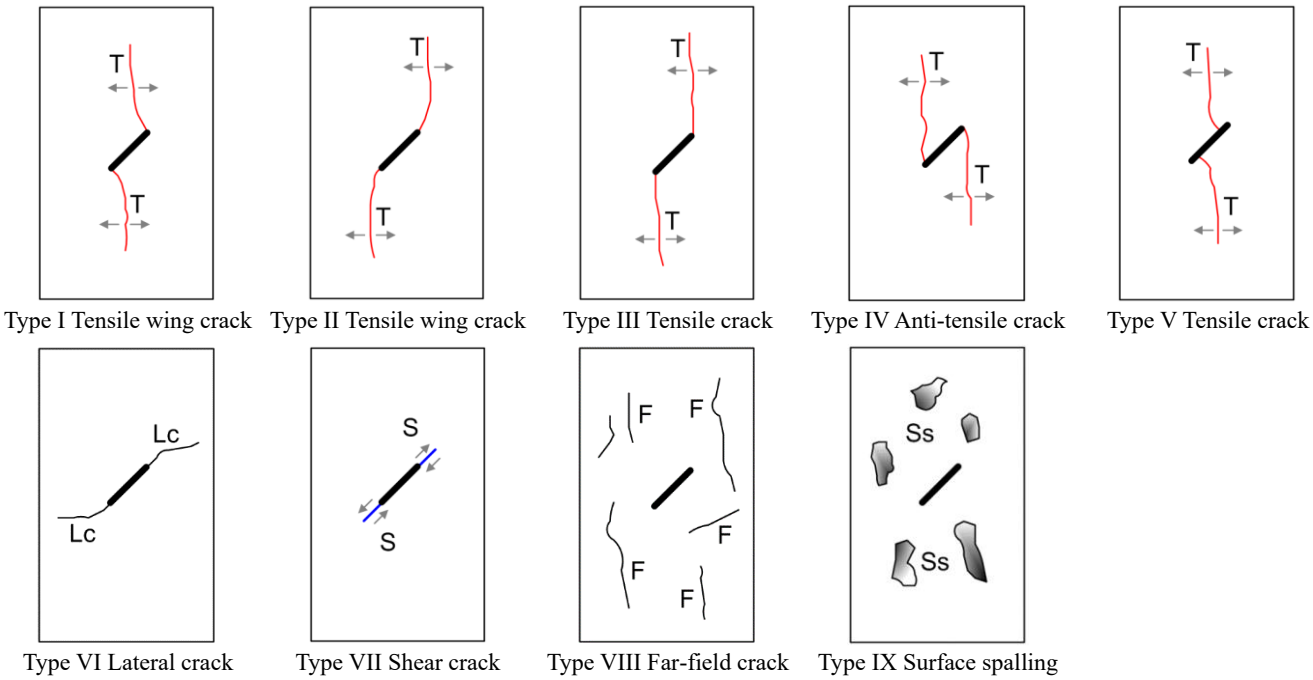

Fig. 11 Different types of cracks observed in sandstone specimens having open flaws (adopted from Yang and Jing 2011)

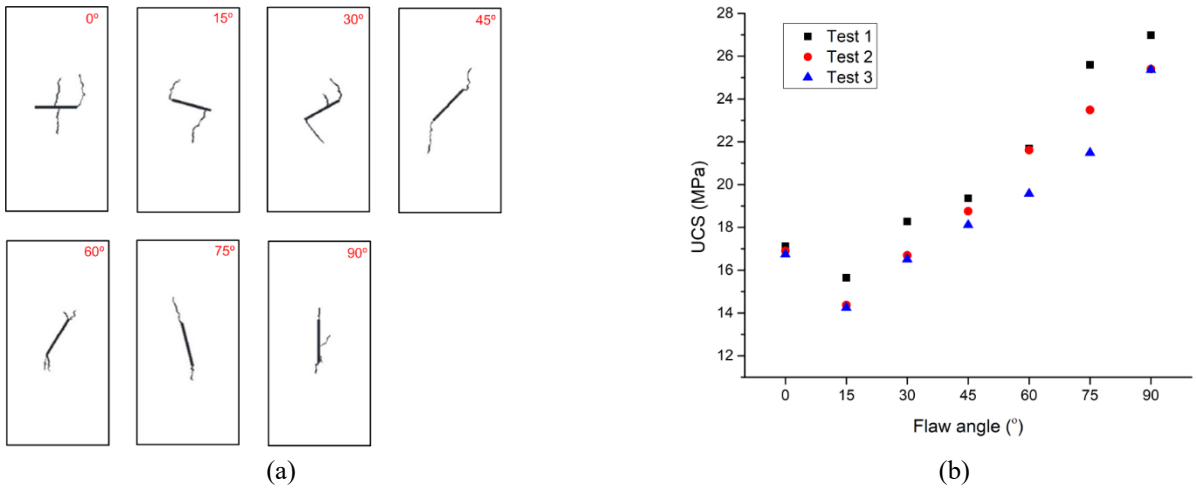

Fig. 12 (a) Geometry of bridge angle between two flaws and (b) Three coalescence modes namely tensile (T) shear (S) and mixed (M) observed in double flaw under uniaxial compression (adopted from Reyes and Einstein 2011)

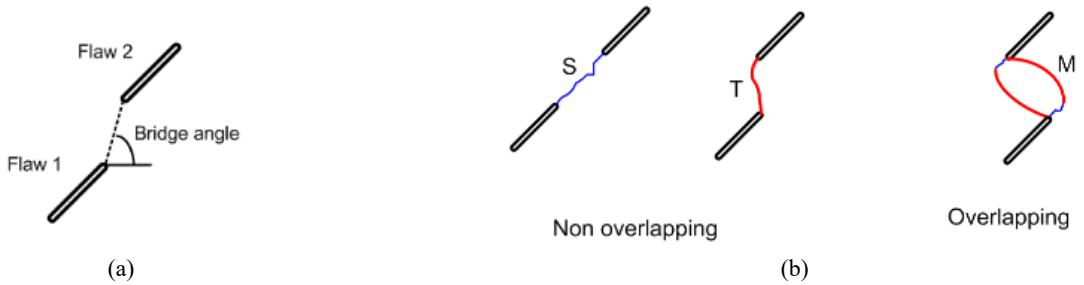

Fig. 13 (a) Geometry of bridge angle between two flaws and (b) Three coalescence modes namely tensile (T) shear (S) and mixed (M) observed in double flaw under uniaxial compression (adopted from Reyes and Einstein 2011)

geometry with three lateral stresses, where wing crack was initiated due to tensile stress concentration at the crack tip.

The initiation position of the wing crack changes from the flaw tip to the middle section of the flaw with an

Type	Coalescence pattern	Coalescence crack type	Lateral stress
I	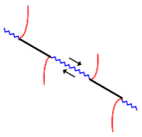	Shear crack	< 2.5 MPa
II	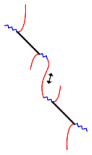	Shear crack and tension crack	< 2.5 MPa
	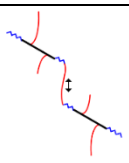		≤ 5 MPa
	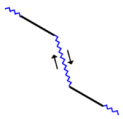		>5 MPa

Fig. 14 Crack coalescence was observed in biaxial compression (adopted from Bobet and Einstein 1998a)

increase in lateral stress and the secondary crack is observed at the flaw tip due to shearing.

The nature of coalescence was further classified using high-speed video by Wong and Einstein (2009b) with gypsum and marble specimens (Fig. 15). They categorized nine types of coalescence mechanisms, which were influenced by flaw angle, bridge angle and spacing between two flaws. Like Reyes and Einstein's study (1991), the nature of coalescence was observed to change from shear to mixed shear-tensile and tensile when the flaw changes from non-overlapping to an overlapping arrangement. However, there was a pronounced difference between gypsum and marble material, where an additional formation of the white patch was observed in marble specimens. Based on the scanning electron microscope (SEM) images, the patches are formed in the region of micro cracking zones before the initiation of a macro cracking process (Fig. 16). After the formation, the shear cracks were immediately preceded and the patches got lengthened and widened, until shear crack gets initiated along with them. In contrast, the development was very limited in gypsum, which is related to the material's textural properties (Wong and Einstein 2009c). The coalescence behaviour was also studied with three flaws and sixteen flaws by Sagong and Bobet (2002) using gypsum specimens. They categorized the coalescence into nine types which vary with flaw arrangements (Fig. 17). From their study, the cracking behaviour observed for multiple flaws can be analogous to two flaws where the cracking phenomenon of tensile and shear cracks was observed to be similar. The secondary cracks were observed to initiate in two directions, either in coplanar or oblique, whereas, the tensile crack initiates oblique to the flaw surface. In addition, the crack initiation stress due to tensile and shear, and subsequent coalescence stress, were affected by the flaw arrangement, flaw angle, and its numbers. It was noted that the crack initiation stress and coalescence stress increase with an increase in flaw angle and spacing. However, the stresses are found to decrease when thenumber of flaws increases. Also, the crack initiation stress, uniaxial compressive strength and peak axial strain for a single flaw are usually higher than combined flaw configurations. The observation was identified on sandstone specimens containing single and combined flaws under uniaxial compression by Yang (2015). The crack evolution process was investigated using photographic monitoring technique. The tensile wing crack was first initiated at the upper and lower tips of the flaw and is often accompanied by anti-tensile cracks. Sarfarzi *et al.* (2021) identified the compressive strength of material found to be increasing with an increase in flaw angle and bridge angle between two echelon non-persistent joints similar to open flaw configuration on concrete specimens. Similar to Sagong and Bobet (2002), the shear-natured failure was observed in the specimen, forming from the number of micro induced tensile cracks. When the joint and bridge angle, the tensile cracks was more pronounced forming tensile failure.

Later Sarfarzi *et al.* (2022) performed the test using acoustic emission (AE) activities where the events at the stage of crack initiation, propagation and coalescence are monitored. In each stage corresponding to every large number of AE hits, the specimen was showing stress drop. Failure behaviour of concrete specimens having five joints under uniaxial compression was studied by Amini *et al.* (2021). The pecimen consisted of two different lengths of parallel and intersecting configurations. The specimen showed dominant compressive failure behaviour with an increase in distance between the inner tips of neighbouring flaws and a decrease in joint length.

Category	Coalescence patterns	Coalescence crack types
I	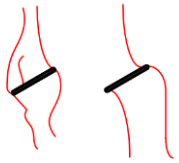	No coalescence
II	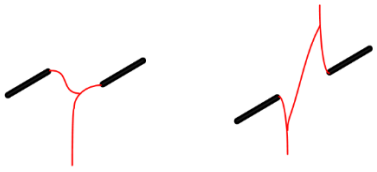	Indirect coalescence by two or multiple cracks
III	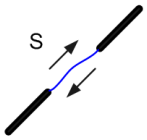	Type 2 S crack
IV	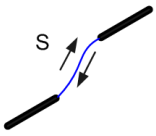	Type 1 S crack
V	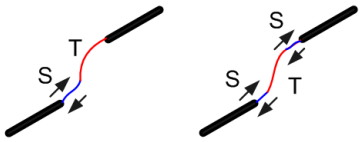	One or more type 2 S cracks and type 2 T crack
VI	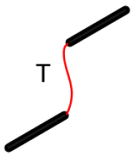	Type 2 T crack
VII		Type 1 T crack
VIII	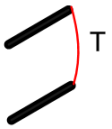	T crack with short segment S crack
IX	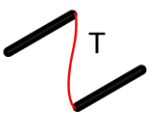	Type 3 T crack

Fig. 15 Types of coalescence observed under uniaxial compression for parallel double flaw (adopted from Wong and Einstein 2009b)

(a) (b)

Fig. 16 (a) Development of white patch observed from SEM for marble specimen are 94% of failure stress and (b) Pattern of white patch shown in dotted lines (adopted from Wong and Einstein 2009c)

Type	Left stepping	Type	Right stepping	Coalescence crack types
I	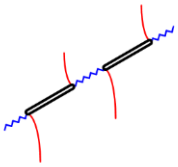	VI	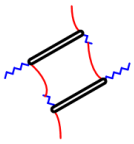	Type I: Quasi-coplanar secondary cracks Type VI: Oblique secondary cracks and wing crack
II	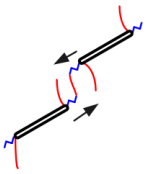	VII	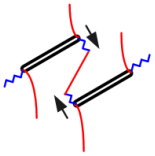	Type II: Quasi-coplanar secondary cracks and out of the plane tensile secondary crack Type VII: Oblique secondary cracks and out of the plane tensile secondary crack
III	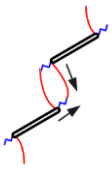	VIII	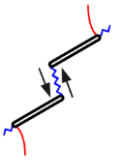	Type III: Quasi-coplanar secondary crack and wing crack Type VIII: Qblique secondary cracks
IV	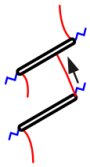	IX	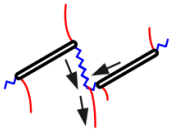	Type IV: Wing crack Type IX: Oblique secondary crack and quasi-coplanar secondary crack
V	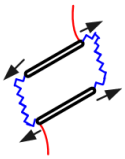			Type V: Quasi-coplanar secondary cracks and out of the secondary shear crack

Fig. 17 Coalescence behaviour was observed with multiple flaws under uniaxial compression (adopted from Sagong and Bobet 2002)

Apart from the parallel flaws, non-parallel flaws in three different materials: PMMA, Diastone and granite were studied by Lee and Jeon (2011). Fig. 18 shows the arrangement of the specimen, a horizontal flaw and an inclined flaw. The inclined flaw was kept underneath the horizontal flaw, and their angles varied from 30° to 90°.

Similar to the parallel flaw, the mode of coalescence observed for a non-parallel configuration was mostly through tensile (T) or tensile and shear (S) cracks. Also, the position of coalescence was found to be shifting with the increase in flaw angle. They analyzed the crack initiation stress and coalescence stress and found that the shielding

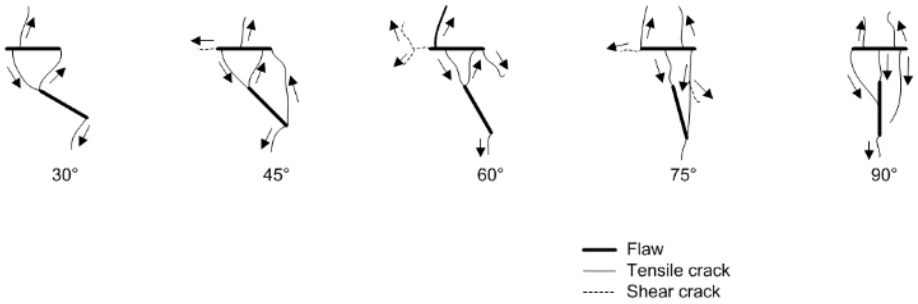

Fig. 18 Coalescence types observed for non-parallel arrangement in diastone specimen (adopted from Lee and Jeon 2011)

effect from horizontal flaw affects the crack initiation and its coalescence behaviour. The effect of crack growth and coalescence behaviour with respect to flaw arrangement in parallel and non-parallel configurations was addressed by Afolagboye *et al.* (2018). They conducted the tests with gypsum specimens having non-parallel configuration by varying the geometrical factors such as ligament length, i.e., the distance between the inner tips of neighbouring flaws and ligament angle is the angle formed between those two flaws with respect to flaw 1 (Fig. 19(a)). The test is carried out by varying the ligament length between two flaws and varying the ligament angle of the flaw (Fig. 19(b)). The nature of crack initiation and propagation were found to be similar with parallel flaw configurations. However, the coalescence mode was observed to change from direct to indirect with an increase in ligament length. No coalescence was recorded between the flaws when the ligament length increased further. Both the studies (Lee and Jeon 2011, Afolagboye *et al.* 2018), noticed the appearance of the wing crack from the flaw tips was not at the same stress level due to uneven stress distribution because of the geometrical arrangement

2.2 Narrow flaw

Literature based on rock fracture identifies the inherent cracks was due to the formation of fracture that exists within the grain boundaries (Brace 1961), and these fractures are often considered elliptical openings. They were assumed to get closed under the compressive loading where closure of the surfaces occurs prior to the tensile crack from the flaw tip. The mechanism of the closed fracture was studied by Hoek and Bieniawski (1965) using glass, where the crack initiation and propagation patterns were studied photo elastically. Under uniaxial compression, the crack is initiated by the relative movement between the flaw surfaces rather than the flaw tip region (Fig. 20). Based on the concept of Modified Griffith theory by McClintock and Walsh (1962), the shear stress parallel to the flaw surface should exceed the shear resistance due to contact between the flaw surface, which later causes the relative movement between the surfaces. The tensile crack was observed on the tensile stress zone due to surface irregularities between the surfaces.

The effect of crack growth and the coalescence pattern, when the flawed surface comes in contact were first studied by Shen *et al.* (1995) on gypsum specimens. The study was conducted on two flaws having parallel configurations whose flaw angle (β°) and bridge angle (α°) are varied. The preparation of open flaw in cast specimen was straightforwardly created by inserting thick metal slots of thickness ≈ 1 mm, In case of closed or narrow flaw conditions they discussed four methods to produce the flaw, namely: (a) Fracturing by impact (‘guillotine’), (b) preinstallation of wax paper in the fracture and leaving in the specimen, (c) back and forth movement of thread during curing and (d) preinstallation of polyethylene and removal after curing. In their experiment, the flaw was installed using a polyethylene sheet of thickness ≈ 0.1 mm. The nature of coalescence for both open and closed flaws was found to depend on the bridge angle between two flaws.

The coalescence mode changes from shear-type for low bridge angle, tensile type for high bridge angle and mixed tensile-shear type for intermediate bridge angles (Fig. 21). Two significant differences were observed, the effect of the curvilinear path reduces compared to the open flaw for the closed flaw and the coalescence stress is observed to be high for closed flaw configuration. Later Wong and Chau (1998) studied the effect of friction between flawed surfaces in sandstone by creating flaws using a stainless-steel sheet with different roughness. Apart from the flaw angle and bridge angle, the mode of coalescence found to depend on the material's friction coefficient (μ). The cracking behaviour was observed to be similar under the same geometry, but the coalescence types observed with open flaws may not be the same as those observed for closed flaws (Fig. 22). Based on the study by Shen *et al.* (1995), the wing crack was deviating away from the main crack. The study reveals that the increased friction coefficient will reduce the angle of deviation from the pre-existing crack (Fig. 23). Also, the peak strength of the material found to increase with increase in friction coefficient and for high flaw angles the strength is found to be independent of the bridge angle. A comparison study between open and closed flaws under uniaxial and biaxial loading conditions was performed by Bobet and Einstein (1998a) on a gypsum specimen with a parallel flaw of non-overlapping configuration. The crack stresses at different stages from initiation of wing crack, secondary cracks, the subsequent coalescence, and failure stress were monitored. The results show that the closed flaw exhibits higher crack stresses than the open flaw. Unlike open flaw, the wing crack gets to initiate after the closure and slippage between the flaw

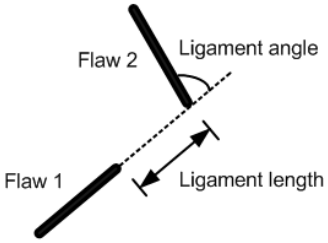

(a)

Coalescence pattern	Coalescence types
	Tensile crack coalescence
	Shear crack coalescence
	Mixed tensile-shear crack coalescence
	Indirect crack coalescence
	No coalescence

(b)

Fig. 19 (a) Flaw configuration defined by ligament length and ligament angle and (b) Additional coalescence was observed for another non-parallel arrangement (adopted from Afolagboye *et al.* 2018)

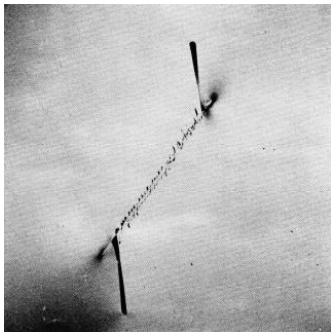

Fig. 20 Crack propagation was observed from a closed flaw in glass (after Hoek and Bieniawski 1965)

surfaces. However, the appearance of the wing crack was observed at the flaw tip irrespective of flaw type (open/closed).

To understand the nature of local strain concentration at the flaw tips, Zhao *et al.* (2016) studied the stress-strain behaviour on cement mortar having double flaw in parallel arrangement. The flaws were prepared from thin metallic sheets of 0.3 mm thickness. The specimens are mounted with strain gauges near the inner tip of the flaw and nearby flaw surface region. A local tensile strain concentration at the flaw tip was found responsible for the occurrence of

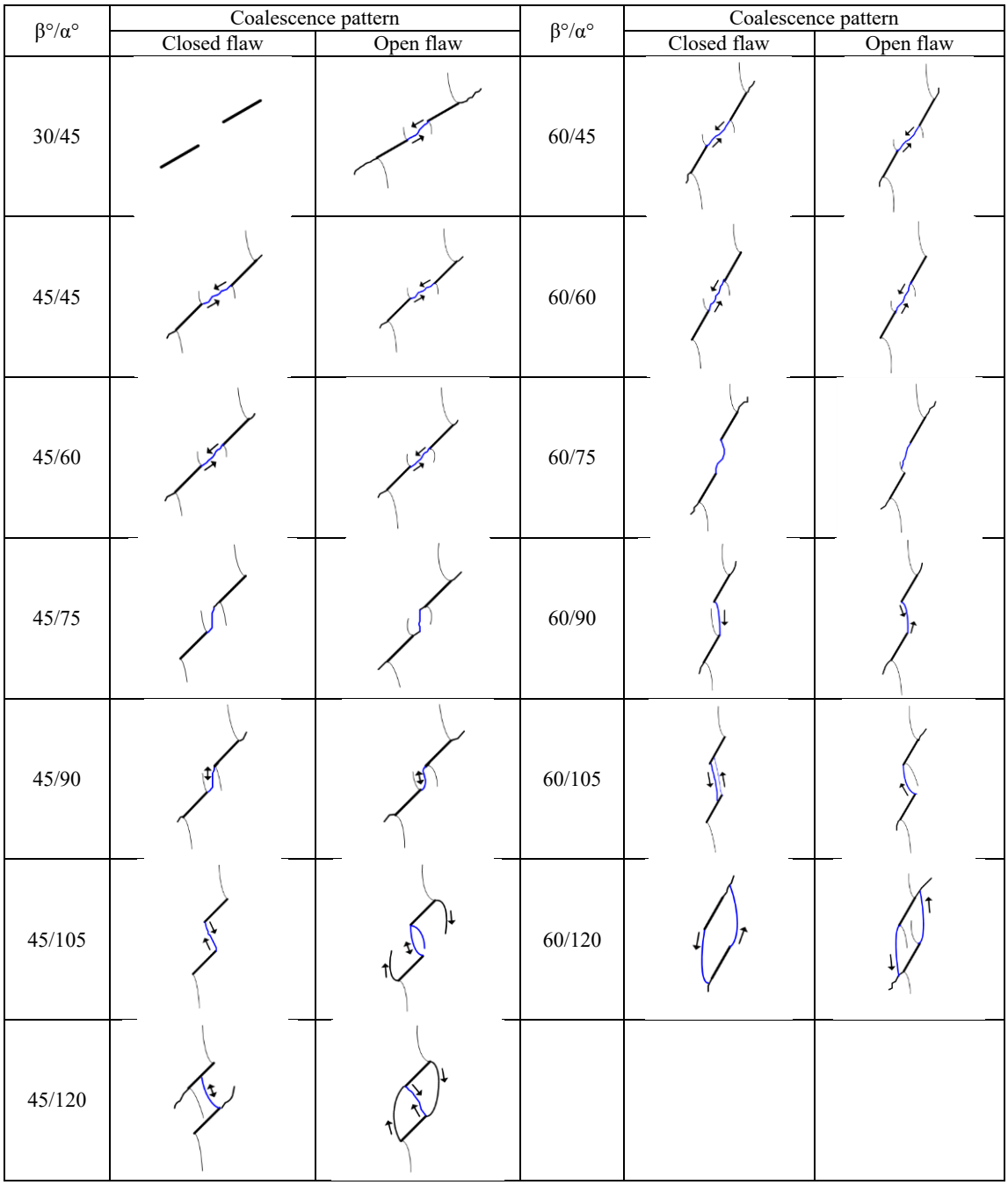

Fig. 21 Types of crack coalescence patterns observed among closed and open flaws for different flaw geometries (adopted from Shen *et al.* 1995)

wing crack and the local compressive strain concentration leads to shear crack. The jump in the local strain indicates the crack growth stability after initiation of cracks. For wing cracks, only a few jumps were observed causing a stable crack growth, whereas in the case of shear cracks a large number of jumps with abrupt compressive strain causes the crack to propagate in an unstable manner leading to specimen failure. The crack stresses for narrow flaw configuration show different stress behaviour when the flaw angle increases (Sivakumar and Maji 2018, 2021). Based on experiments on three different material strengths (15 MPa, 30 MPa and 60 MPa), the study reveals that stresses initially decrease the minimum value around the flaw angle of 45° and increase in flaw angle (Fig. 24).

The mode of tensile crack growth changes from wing tensile crack (T1) in low angle to mixed tensile–shear crack (T1&T2) for intermediate flaw angles (30°- 60°) and coplanar tensile crack (T2) for high flaw angle (Fig. 25). The difference between the crack initiation and peak stresses were found to be lower for low and high flaw angles compared to intermediate flaw angles. The tensile crack from low and high angles usually gets initiated directly towards the direction of the compressive loading and reaches its peak limit. Anti-wing/tensile crack (T3) was observed for high strength gypsum material with the flaw angle of less than 45° and fewer shear cracks than low and

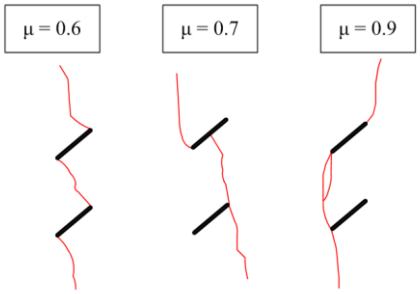

Fig. 22 Change in crack coalescence due to variation in friction (μ) of material (adopted from Wong and Chau 1998)

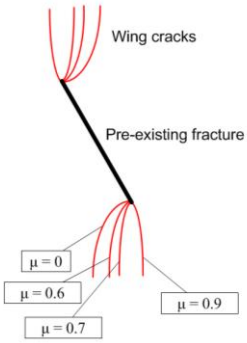

Fig. 23 Crack propagation pattern when flaw surface friction is varied observed by Shen *et al*. (1995)

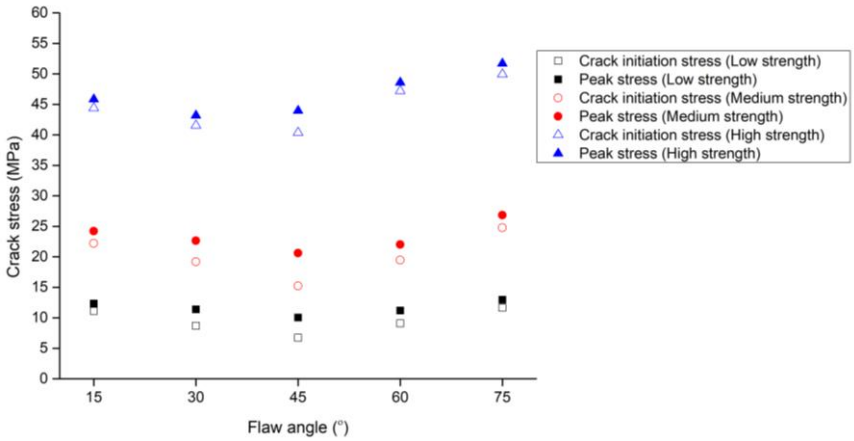

Fig. 24 Crack stress behaviour for different flaw angles on three material strengths (after Sivakumar and Maji 2018)

medium material strength. Further, the effect of narrow on double flaw having non-parallel arrangement using low strength gypsum was studied (Fig. 26) and specimen geometry was made similar to Lee and Jeon (2011) study. In this configuration, the crack propagation pattern due to closure between the flaw surfaces was found to alter the coalescence position. The shielding effect from the horizontal flaw found to influence the increase in crack stresses in the inclined flaw. The difference between the initiation and coalescence stresses reaches minimum at 45° but later increases when the flaw angle increases. Similar to the observations made by Lee and Jeon 2011, Afolagboye *et al.* 2018), the appearance of wing cracks was not observed at all flaw tips for the same stress level. It is also to be noted that further studies are required on non–parallel configurations on narrow flaws under the combination of different geometrical arrangements. The study could lead to more information on coalescence behaviour changes due to friction between the flaws and their corresponding failure behaviour. Further, very limited studies on biaxial compression for narrow flaws were conducted to study the crack propagation pattern's influence and stress behaviour under the complex geometrical combination of flaws.

3. Numerical studies on crack growth

With the advancement in computational techniques, the crack stress behavior and their propagation pattern are extended into numerical methods. Due to the complexity and requirement of advanced instrumentation to capture the crack growth behavior in experiments, the numerical

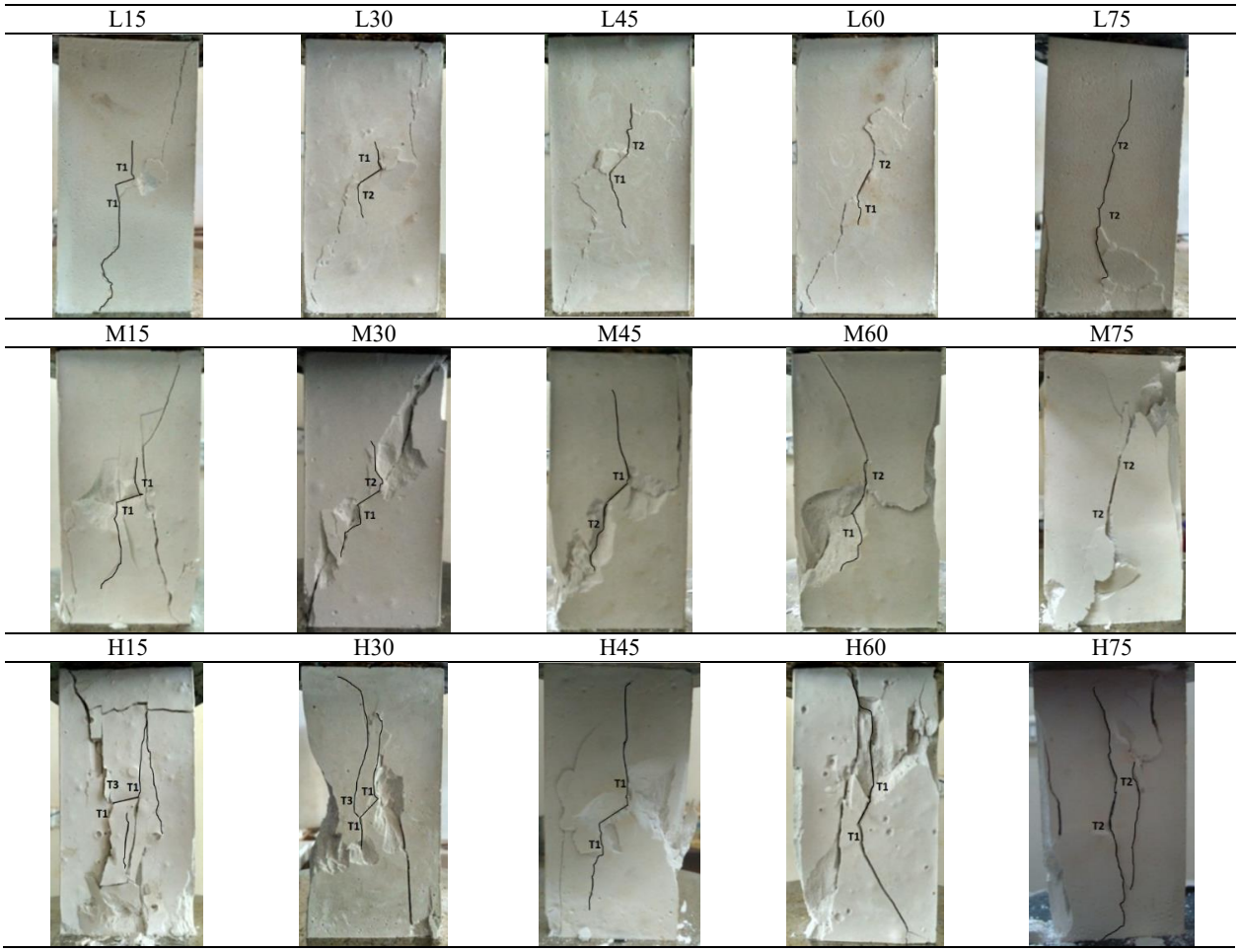

Fig. 25 Crack pattern observed on three different gypsum strengths (a) low (L), (b) medium (M) and high (H) by varying flaw angles (15°, 30°, 45°, 60° and 75°) (after Sivakumar and Maji 2018)

approach can be economical and provide better insight into the cracking process. Various numerical methods like the Finite Element Method (FEM) (Reyes and Einstein 1991, Tang *et al.* 2001, Li and Wong 2012), Extended Finite Element Method (XFEM) (Saberhosseini *et al.* 2014, Xie *et al.* 2016, Sivakumar and Maji 2018, 2021, Haeri *et al.* 2020), Displacement Discontinuity Method (DDM) (Bobet and Einstein 1998b, Vásárhelyi and Bobet 2000), Distinct Element Method (DEM) (Lee and Jeon 2011, Manoucherian and Marji 2012, Zhang and Wong 2012, 2013, Sharafisafa and Nazem 2014, Zhang *et al.* 2015, Sarfarzi *et al*. 2021, 2022, Amini *et al*. 2021), Expanded Distinct Element Method (EDEM) (Zhao *et al.* 2019), Extended non-ordinary state-based peridynamics (NPSB-PD) (Wang *et al.* 2016), Coupled peridynamics-finite element method (PD-FEM) (Lee and Hong 2018), General Particle Dynamics (GPD) (Bi *et al*. 2016), Numerical Manifold Method (Wu and Wang 2012, Kang *et al.* 2022) and Discontinuous Deformation Analysis (DDA) (Wang *et al.* 2021, Wang and Wang 2022) are used to study the crack initiation and propagation by different criteria. In the present study, the scope is limited for discussion of crack growth behaviour based on the above numerical approaches rather than focusing on their advantages and limitations with each other. Table 2 summarizes the literature that addresses the study on crack growth for non-persistent fractures using numerical techniques.

3.1 Open flaw

The crack mechanism of the tensile and shear crack initiation was studied by Reyes and Einstein (1991) by analyzing the stress and strain field around the flaw tip on double flaws having non-overlapping geometries. The study was carried out using the finite element model, ABAQUS, and coalescence behaviour were compared with their experimental results on gypsum specimens. The model adopts the strain-based smeared crack approach with a stiffness degradation model to simulate the crack coalescence. Based on major tensile principal stress and strain contour from their analysis, the formation of tensile crack was observed at the flaw tip and bridges only at the higher tensile strain doted region rather than the higher stress doted region (Fig. 27(a)). However, the strain-based criteria predict large tensile and compressive principal stresses exhibited in the higher principal strain doted region (Fig. 27(b)). The adopted approach can model the secondary and coalescing cracks, however, it is also valid in predicting the tensile crack at the flaw tip (Bobet 1997).

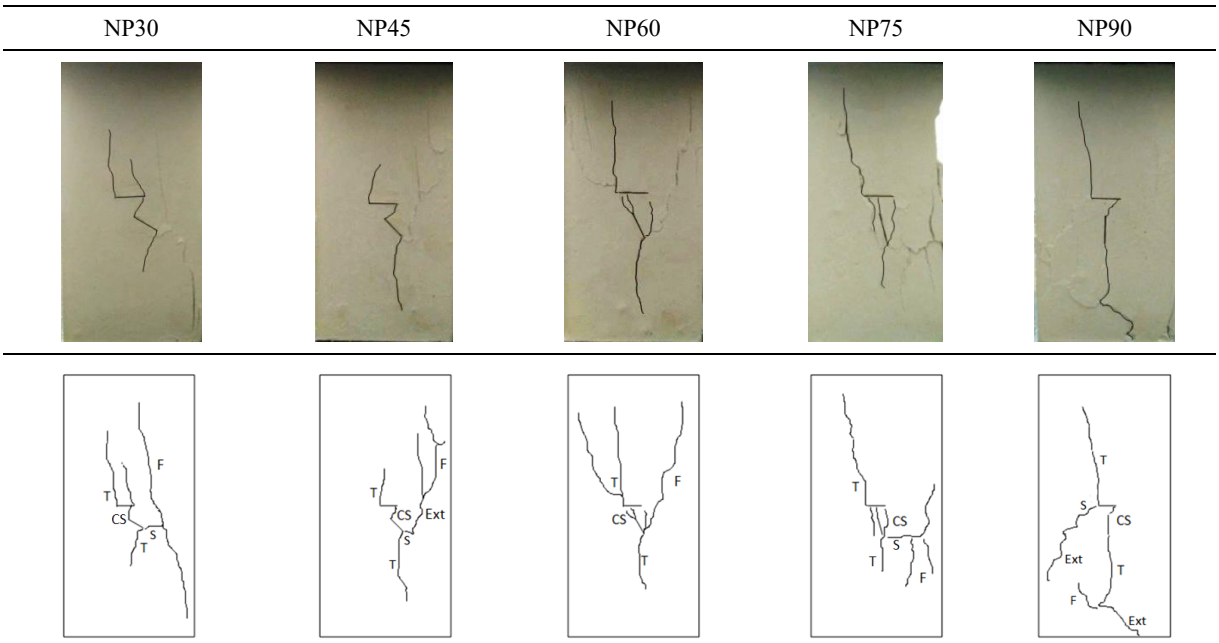

Fig. 26 Coalescence behaviour was observed for non-parallel (NP) double flaw configuration based on tensile (T), shear (S), coalescence (CS), far-field (F) and extension (Ext) cracks (after Sivakumar and Maji 2021)

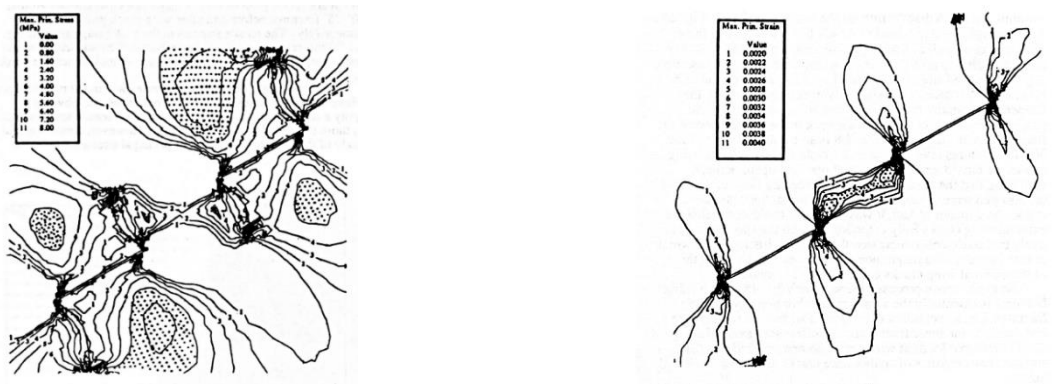

(a) (b)

Fig. 27 Simulated crack and coalescence for specimen of 30° flaw angle and 45° bridge angle based on (a) Maximum tensile principal stress and (b) Maximum tensile principal strain contours (after Reyes and Einstein 1991)

Later, a numerical study by Bobet and Einstein (1998b) assumed the tensile cracks to initiate in the direction perpendicular to the maximum tensile tangential stress region from the flaw tip. The shear cracks were assumed to initiate at the maximum shear stress region from the flaw tip. The numerical model was based on the Displacement Discontinuity Method using FROCK code. The crack growth simulated from the adopted model was compared with their experiments with respect to initiation, propagation and coalescence of parallel double flaws from their experiments using gypsum. Though the predicted crack initiation and propagation based on stress-based criteria were found to be less precise, it was acceptable with experimental results (Fig. 28). The numerical analysis indicated that the wing crack initiation stress increases with an increase in flaw angle, ligament length and confining stress. The coalescence stress was observed after wing cracks initiation stress. However, the model considered the presence of flaws only in an infinite medium. The actual specimen and its boundaries effect were considered later by Vásárhelyi and Bobet (2000). From their study, the tensile cracks and secondary shear cracks were observed initiating at the same stress level irrespective of flaw geometry. According to their analysis, the wing cracks initiate perpendicularly to the secondary shear cracks and grow in the most compressive direction (Fig. 29(a)). The shear cracks propagate at approximately 45° with the uniaxial cracks and secondary shear cracks were observed initiating at the same stress level irrespective of flaw geometry. According to their analysis, the wing cracks initiate perpendicularly to the secondary shear cracks and grow in the most compressive direction (Fig. 29(a)). The shear

Table 2 Literatures adopted in the present study using different numerical approaches

Material adopted	Flaw type	Geometry	References
Uniaxial compression			
Marble	Open	Single flaw	Li and Wong (2012) – Finite Element Method
Sandstone	Open and filled flaw	Single flaw	Wang and Wang (2022) – Discontinous Deformation Analysis
	Closed	Three flaw (parallel)	Tang *et al*. (2001) – Finite Element Method
Granite	Open	Single flaw and double flaws (non-parallel)	Lee and Jeon (2011) – Distinct Element Method
Gypsum	Open	Single flaw	Zhang and Wong (2012) – Distinct Element Method Wu and Wang (2012) - Numerical Manifold Method
		Double flaw (parallel)	Reyes and Einstein (1991) – Finite Element Method Zhang and Wong (2013) – Distinct Element Method Kang *et al*. (2022) – Numerical Manifold Method
		Double flaw (non-parallel)	Zhang *et al.* (2015) - Distinct Element Method Kang *et al*. (2022) – Numerical Manifold Method
		Multiple random flaws	
	Open and Closed	Double flaw (parallel)	Bobet and Einstein (1998b), Vásárhelyi and Bobet (2000) – Displacement Discontinuity Method
	Closed	Single flaw and double flaws (non-parallel)	Sivakumar and Maji (2018, 2021) – Extended Finite Element Method
Concrete	Open	Three flaws (parallel)	Sarfarazi *et al.* (2021, 2022) – Distinct Element Method
		Five flaws (parallel and intersecting)	Amini *et al.* (2021) – Distinct Element Method
Model rock	Open	Double flaw (non-parallel)	Lee and Hong (2018) – Coupled Peridynamics – Finite Element Method
	Closed	Single flaw	Xie *et al*. (2016) – Extended Finite Element Method
	Open and Closed	Double flaws (parallel)	Sharafisafa and Nazem (2014) – Distinct Element Method
Cement mortar	Open	Single flaw	Wang *et al*. (2021) – Numerical Manifold Method
Biaxial compression			
Model rock	Open	Single flaw	Manoucherian and Marji (2012) – Distinct Element Method
Gypsum	Open	Single flaw	Zhao *et al*. (2019) – Expanded Distinct Element
		Double flaw (parallel)	Wang *et al.* (2016) – Extended non-ordinary state peridynamics
		Four flaw (parallel)	Bi *et al.* (2016) – General Particle Dynamics
	Open and Closed	Double flaw (parallel)	Bobet and Einstein (1998b) – Displacement Discontinuity Method
	Closed	Single, Double and Three flaws (parallel)	Haeri *et al.* (2020) – Extended Finite Element Method

cracks propagate at approximately 45° with the uniaxial and they decrease with an increase in flaw angle.

The systematic behaviour of crack coalescence in single and double flaws having non-parallel configurations, was studied by Lee and Jeon (2011) for granite specimens using Particle Flaw Code (PFC^{2D}), a distinct element method (DEM). Under a single flaw specimen, the crack initiation and propagation direction for intermediate angles (30° - 60°) were observed towards the major compressive stress loading. When the flaw angle exceeds 75°, the crack propagation found to deviate from the major compressive stress direction and specimens failed like a shear plane (Fig.

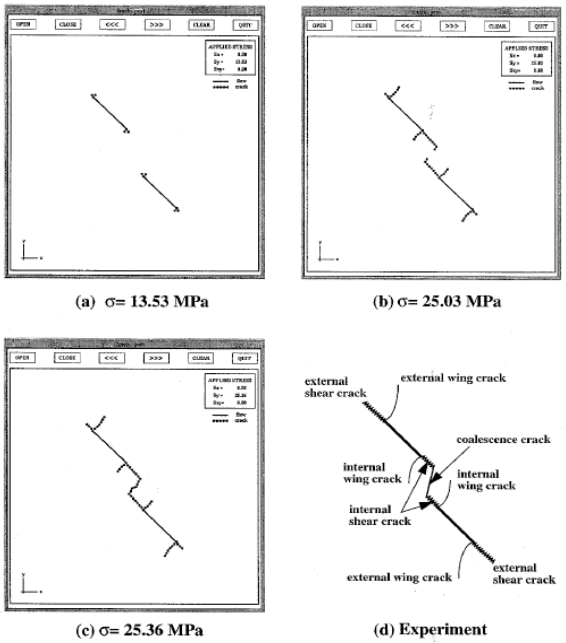

Fig. 28 Predicted crack growth behaviour based on FROCK with experimental pattern (after Bobet and Einstein 1998b)

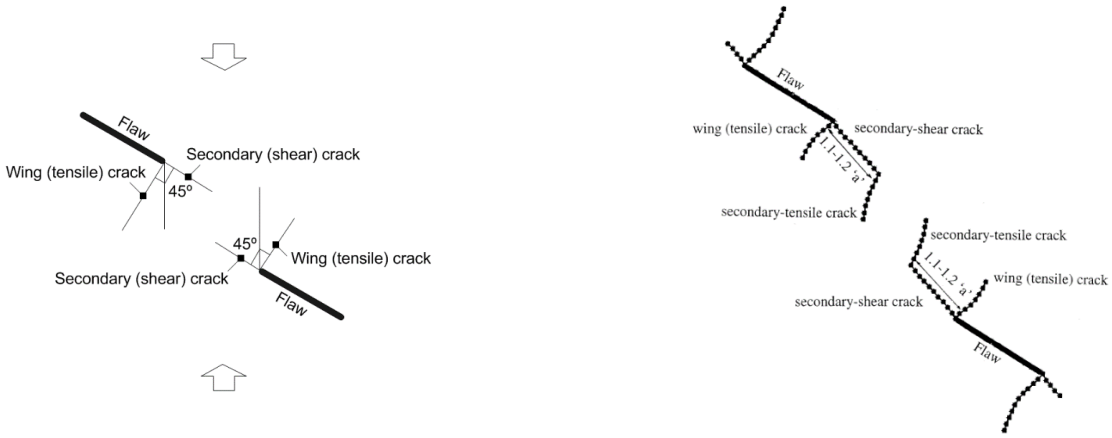

(a) (b)

Fig. 29 Initiation direction of tensile and shear cracks and direction during propagation obtained from numerical model (after Vásárhelyi and Bobet 2000)

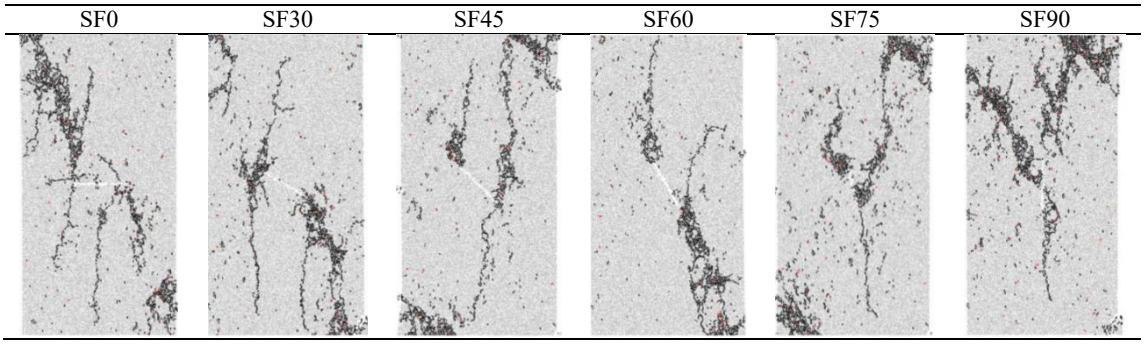

Fig. 30 Crack pattern observed for single flaw (SF) granite specimen between experiments and PFC^{2D} numerical model where tensile and shear cracks represented by black and red dots (after Lee and Jeon 2011)

30). In the case of double flaw arrangement, for inclined flaw at 30°, two cracks were observed from the right tip where one of the cracks grew towards the specimen's side (Fig. 31). For the flaw angle between 45° - 75°, the

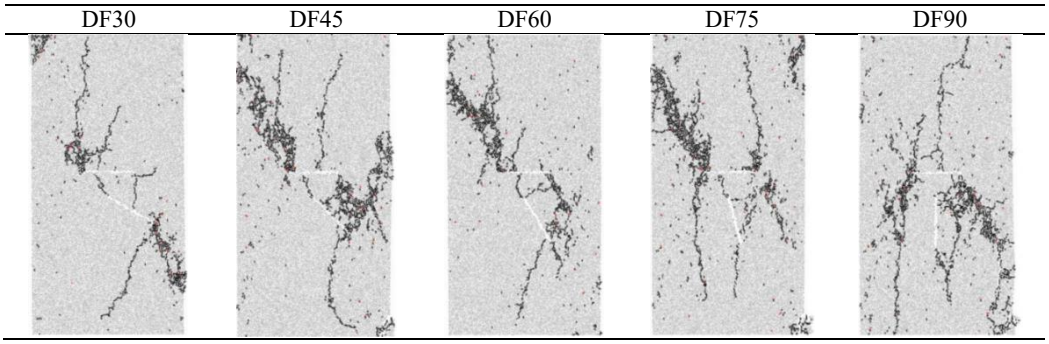

Fig. 31 Crack coalescence behaviour was observed for double flaw (DF) granite specimen between experiments and PFC^{2D} numerical model where tensile and shear cracks were represented by black and red dots (after Lee and Jeon 2011)

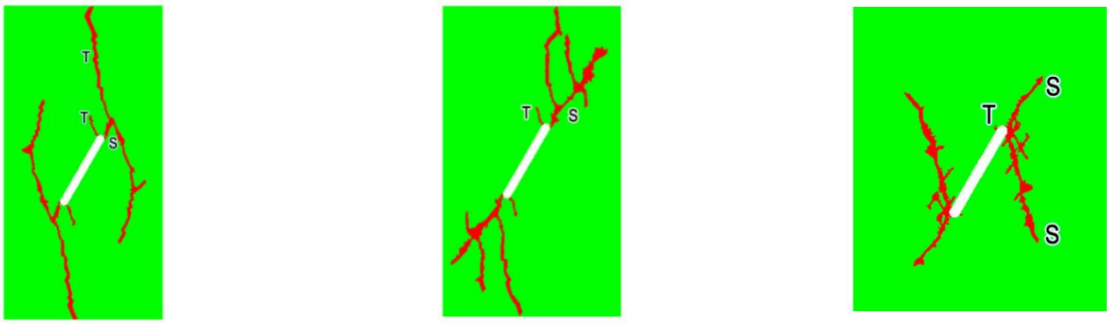

(a) (b) (c)

Fig. 32 Crack initiation and propagation were observed under (a) low, (b) medium and (c) high loading rates (after Li and Wong 2012)

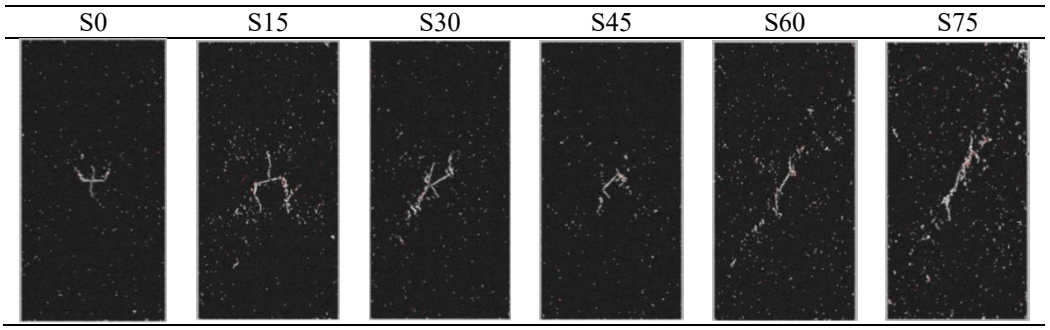

(a)

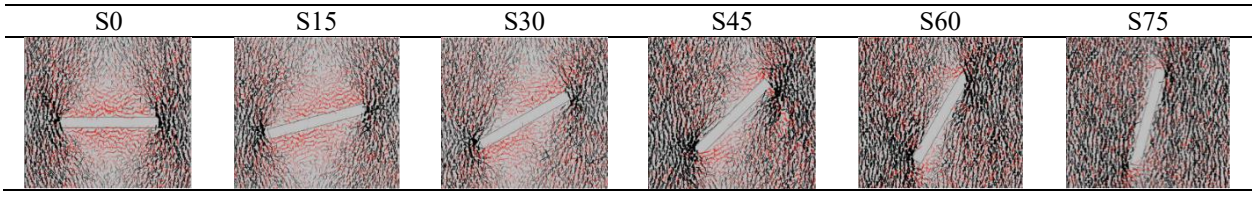

(b)

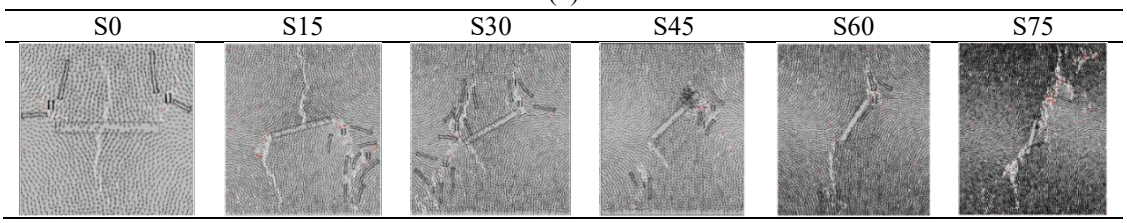

(c)

Fig. 33 (a) Cracking behaviour, (b) Stress analysis and (c) Deformation analysis observed from PFC model where red colour indicates tensile, black for compressive and white batch shows formed micro tensile cracks (after Zhang and Wong 2012)

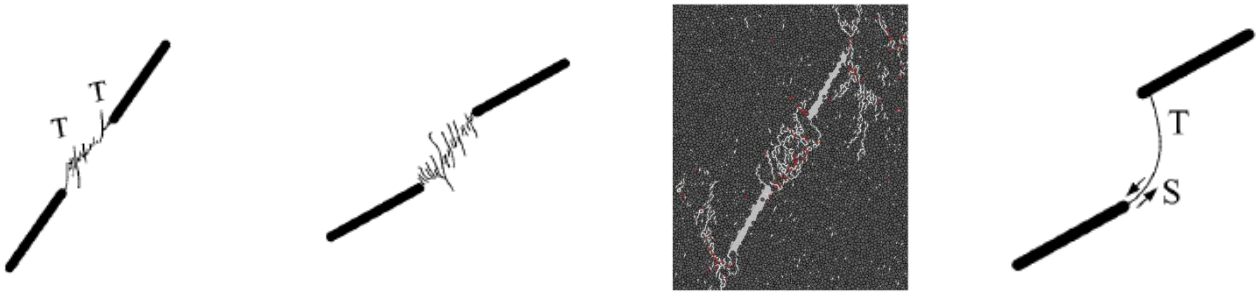

(a) (b) (c)

Fig. 34 (a) New coalescence type 1 was observed on coplanar double flaw, (b) Formation of shear band (red colour) from macro tensile cracks (white colour) and (c) New coalescence observed for stepped double flaw (after Zhang and Wong 2013)

(a) (b)

Fig. 35 All three modes of crack (I-tensile, II-shear, I-II mixed) captured using NMM for (a) double flaw and (b) Multiple random distributed flaws (after Kang *et al*. 2022)

coalescence was observed forming between the horizontal and inclined flaws at the left and right tips. Also, the crack from the left tip of the horizontal flaw was found propagating upwards but away from the major loading direction to the left corner of the specimens. Based on study by Lee and Hong (2018), the failure pattern in non-parallel flaw configurations was also found to be influenced by the overlapping ratios between two flaws. They investigated the systematic behaviour of crack coalescence in rock using a parallelized peridynamics formulation coupled with a finite element method (PD-FEM). From their study, an additional formation of x-shaped band was observed in addition to formation of tensile and shear cracks which influences the failure pattern of the material. Further, the formation of crack types and propagation behaviour were not influenced by the geometrical arrangement but also by the loading rate. Later, Li and Wong (2012) studied the cracking behaviour on marble specimens under three different loading rates using FEM-based software ANSYS. The numerical model was performed for a single flaw based on material properties by Wong and Einstein (2009a) (Fig. 32). The tensile cracks were found to initiate before shear cracks under slow loading rate whereas under high loading rate shear cracks observed before the tensile cracks. Also, the crack pattern under a slow loading rate shows different behaviour than the high-speed loading rate. From their simulation, tensile cracks (T) were found to initiate close to the flaw center for low flaw angles, and their position shifts toward the flaw tip region for large flaw angles. Irrespective of flaw inclination, the shear crack (S) position is observed only at the flaw tip region.

Based on stress and displacement analysis of the PFC model by Zhang and Wong (2012) from Wong and Einstein's (2009a) experiments on a single flaw, a higher compression at the tip and tension distribution around the flaw surface perimeter was observed for shallow flaw angles of 0° and 15° (Fig. 33(b)). With the increase in the flaw angle, the tension distribution becomes narrower and found to move towards the flaw tip whereas the compressive force concentration found to surround the flaw surface. The change in force distribution was reflected in the crack initiation position where the crack found to initiate at the flaw tip when the angle increases (Fig. 33(a)). From the displacement analysis, the first cracks developed from the flaw were usually by the dominant micro tensile crack. In contrast, the secondary cracks were found to develop from a higher portion of micro shear cracks. At low flaw angles, the first crack initiated was tensile in nature, followed by the secondary crack in shear nature which occurs coplanar or quasi direction with the first crack. When the flaw angles increase, especially at 75°, the secondary crack observed initiation along the path of the

Flaw geometry	Coalescence pattern	Coalescence type
α = 135°	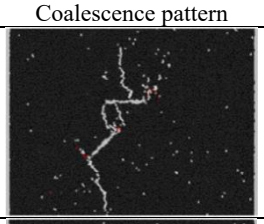	Tensile crack with shear coalescence at tip
α = 90°	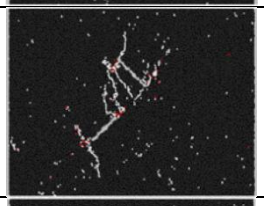	Mixed (tensile-shear) and indirect crack linkage
α = 45°	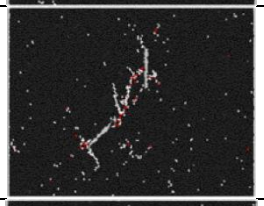	Indirect and shear crack linkage
α = -45°	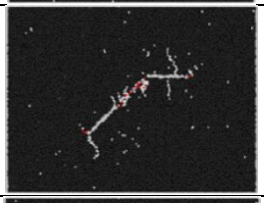	Mixed (tensile-shear) and shear crack linkage
α = -90°	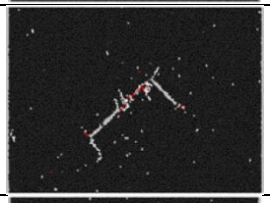	Mixed (tensile-shear), indirect and shear crack linkage
α = -135°	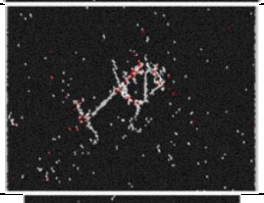	Mixed (tensile-shear) and indirect crack linkage
β = 60°	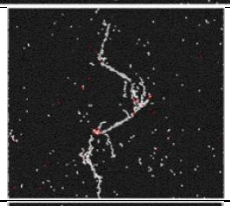	Tensile and indirect crack linkage
β = 45°	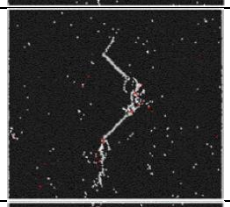	Mixed (tensile-shear), indirect and tensile crack linkage
β = 30°	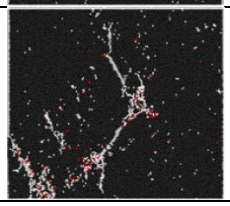	Mixed (tensile-shear) and indirect crack linkage

Fig. 36 Types of crack coalescence observed for non-parallel double flaw for underneath and partially underneath configurations (after Zhang *et al*. 2015)

first crack (Fig. 33(c)). Subsequently, Zhang and Wong (2013) studied the crack coalescence behaviour on double flaws having parallel configurations limiting it to non-overlapping geometries. From their analysis, two additional coalescence types were identified apart from nine types of coalescence observed by Wong and Einstein's (2009b) experiments (Fig. 15). The coalescence was formed between two inner flaw tips by linkage of the number of steeply inclined vertical macro-tensile cracks instead of single macro-cracking trending with coplanar geometry (Fig. 34(a)). The cracks later develop as a shear band when the loading increases (Fig. 34(b)). For stepped flaw geometry, the coalescence was formed by the linkage between two inner flaw tips - one of tensile nature and another of mixed tensile-shear nature (Fig. 34(c)). Later, Kang *et al*. (2022) identified the orientation of the initiated tensile cracks could be captured more efficiently for the same experiment by numerical manifold method (NMM). The adopted method could simulate the crack by continuum and discontinuum using mohr-coulomb and maximum tensile stress criterion in a unified network without additional enrichment. The model found suitable for simulating the fractures in the specimen for all mode I (tension), mode II (shear) and mixed mode I-II conditions (Fig. 35(a)). Further, they investigated crack growth behaviour for rock having multiple random distribute cracks configuration where the crack position, direction and propagation path of cracks are well defined (Fig. 35(a)).

The stress distribution for non-parallel configuration was more complicated than parallel flaw configuration, which affects the crack initiation and coalescence based on Zhang *et al*. (2015). In their study using the bonded-particle model (BPM), a distinct element-based model, they analyzed the experiment study of Zhang and Wong (2012) having non-parallel flaws by varying flaw angle (α) and bridge angle (β) between them. The previous studies have categorized the crack coalescence into nine types based on two flaws arranged in a parallel configuration. Their study observed the difference in crack coalescence type in non-parallel flaw arrangement and distinguished them based on the tensile/shear nature (Fig. 36). Their study observed that the flaw bridge angle influences the crack growth and coalescence pattern. Coalescence is most commonly observed in the configuration where one flaw is underneath the other. Under the influence of confinement, though wing and shear crack initiates at the same stress level, for double flaw having non-overlapping geometry, the material failure is influenced by the shear crack (Bobet and Einstein 1998b). From Fig. 37, based on the FROCK model, the initiated shear cracks are usually found to propagate in an unstable manner in coplanar or quasi-coplanar. They later get deviated towards the inner tips of the flaw, usually forming immediate coalescence with adjacent/neighboring cracks. Based on the PFC model on a single flaw by Manoucherian and Marji (2012), the initiation direction of secondary crack was influenced by the confining stress. The tensile cracks are initiated from the particle vector contour due to induced tensile stresses at the flaw tips (Fig. 38(a)). When the confinement increases, this induction observed to gets weakened. It closes the tensile cracks and the bond formed

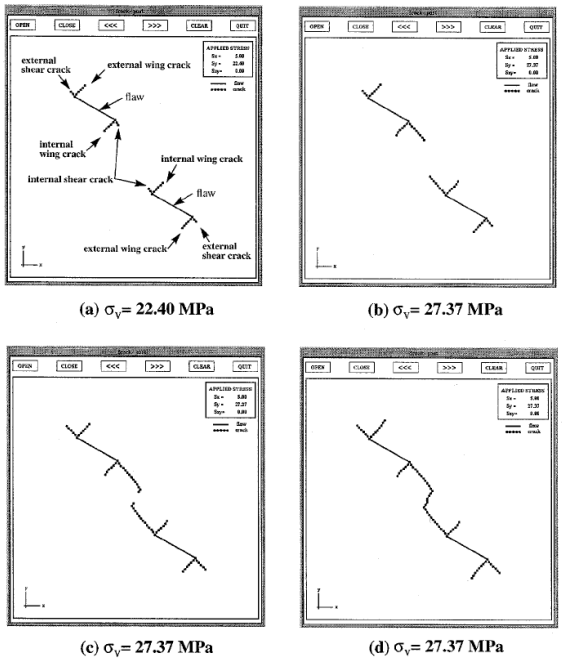

Fig. 37 Coalescence due to shear crack under biaxial compression was observed for open flaw geometry using FROCK (after Bobet and Einstein 1998b)

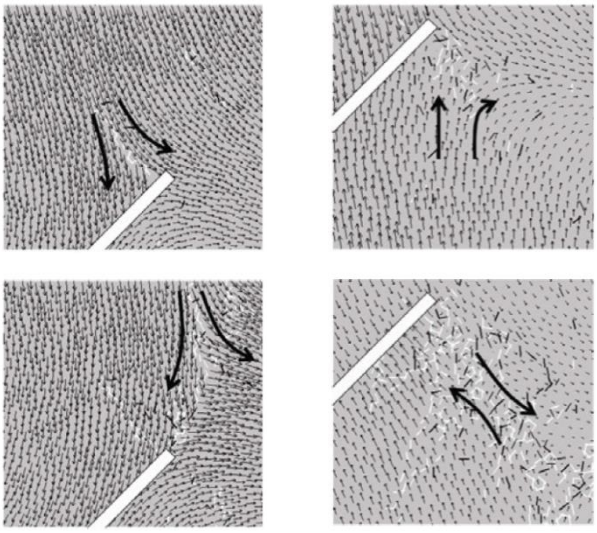

Fig. 38 (a) Formation of tensile cracks due to induced tensile stresses from particle displacement and (b) A new secondary crack when subjected to confinement (after Manoucherian and Marji 2012

by the particles gets broken, forming secondary cracks which propagate later in a different direction (Fig. 38(b)). Also, the secondary cracks are first initiated under the tensile opening; however, under additional loading, it eventually changes to shearing mode. Hence, it would be incorrect to recognize secondary cracks as shear cracks. Subsequently, Wu and Wong (2012) further investigated the nature of crack initiation using NMM based on gypsum specimen from Wong and Einstein (2009a) study under both

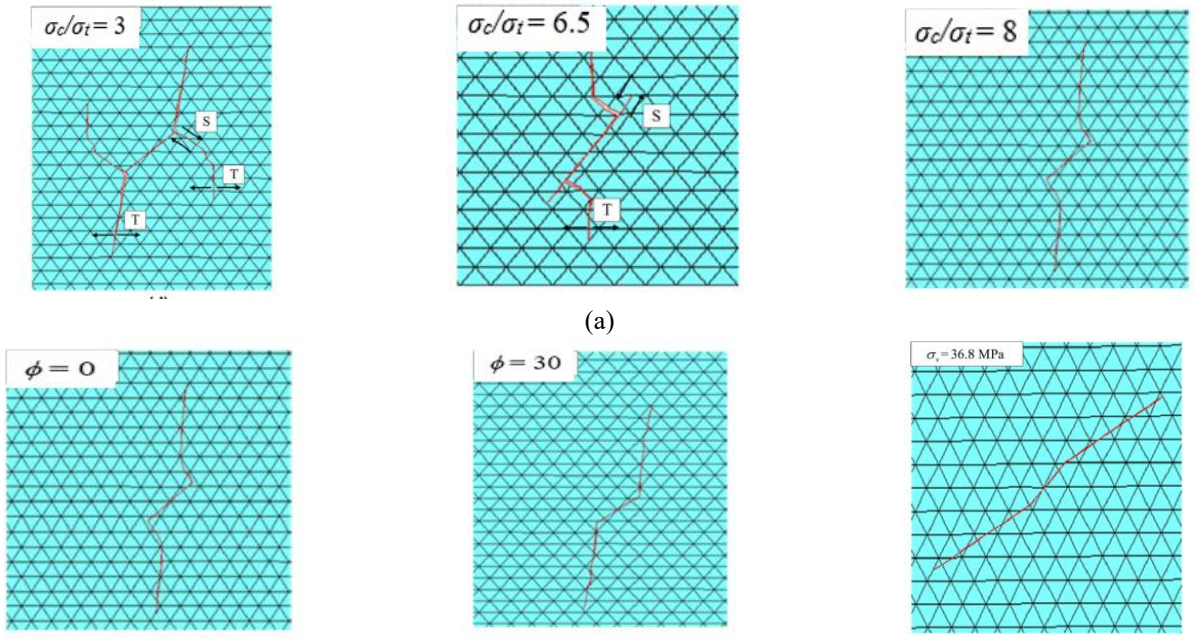

Fig. 39 (a) Shear crack formation with increase in ratio between compressive and tensile strength (σ_c/σ_t) (b) Change of crack from tensile to shear with increase in friction angle (ϕ) and (c) pure shear crack with increase in biaxial compression (after Wu and Wong 2012)

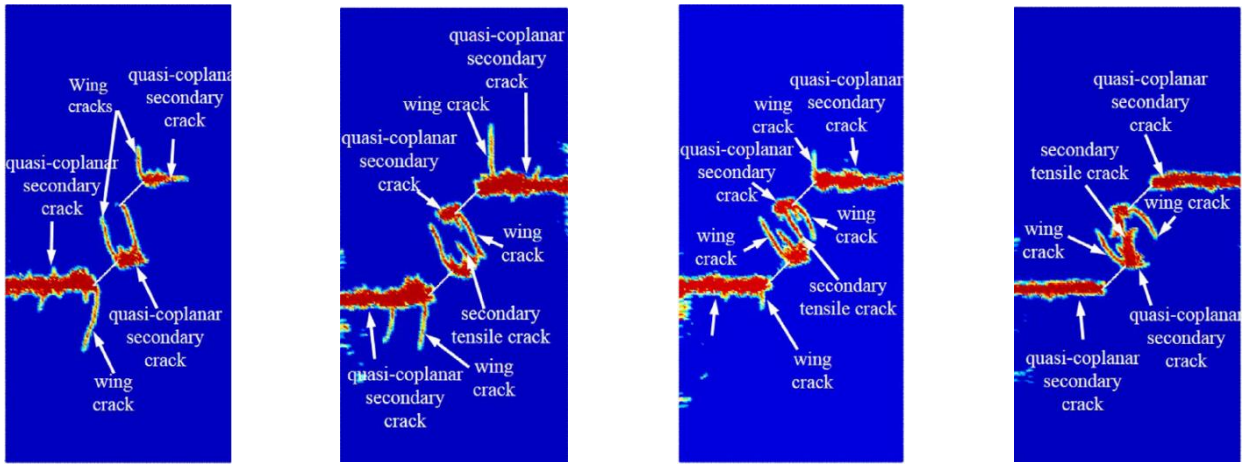

Fig. 40 Failure pattern observed on double flaw non-overlapping geometries for different confinements (a) 2.5 MPa, (b) 5 MPa, (c) 7.5 MPa and (d) 10 MPa (after Wang *et al.* 2016)

uniaxial and biaxial compression. They found that the nature of secondary crack is dependent on the ratio between compressive and tensile strength of the specimen. For lower ratio, shear crack found to initiate first instead of tensile crack (Fig. 39(a)). With increase in friction angle, shear crack found to more favourable to initiate before wing crack (Fig. 39(b)). For biaxial compression, the effect of lateral confining stress leads to a larger crack initiation stress, where the initiation of tensile cracks found to be suppressed (Fig. 39(c)).

Apart from the nature of change in crack propagation, the order of appearance of tensile and shear cracks gets affected by the increase in confinement based on Wang *et al.* (2016) study. They adopted the gypsum material from Bobet and Einstein's experimental study (1998a) and simulated a double flaw having non-overlapping geometry using extended non-ordinary state-based peridynamics. The analysis was performed with four different confinements 2.5, 5, 7.5 and 10 MPa with a flaw angle of 45°, spacing and continuity between two flaws equal to half of the flaw length. For confinement of 2.5 MPa, the coalescence was observed to form between wing crack from the inner tip of both flaws and a quasi-coplanar secondary crack at one of the flaw tips (Fig. 40(a)). In 5 MPa confinement, both wing crack and quasi-coplanar secondary cracks appeared simultaneously at both inner and outer flaw tips. The length

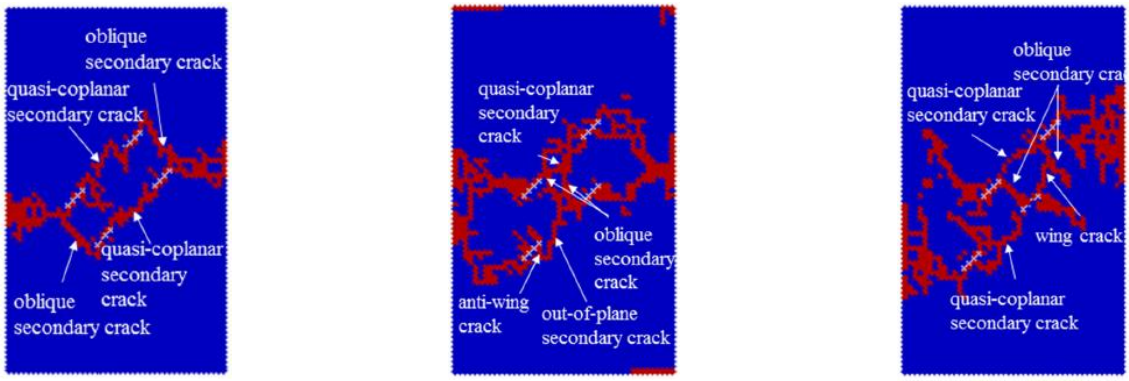

(a) (b) (c)

Fig. 41 Change in coalescence observed on four pre-existing flaws for varying continuity, c (a) c = 0 mm, (b) c = 10 mm and (c) c = 20 mm (after Bi *et al*. 2016)

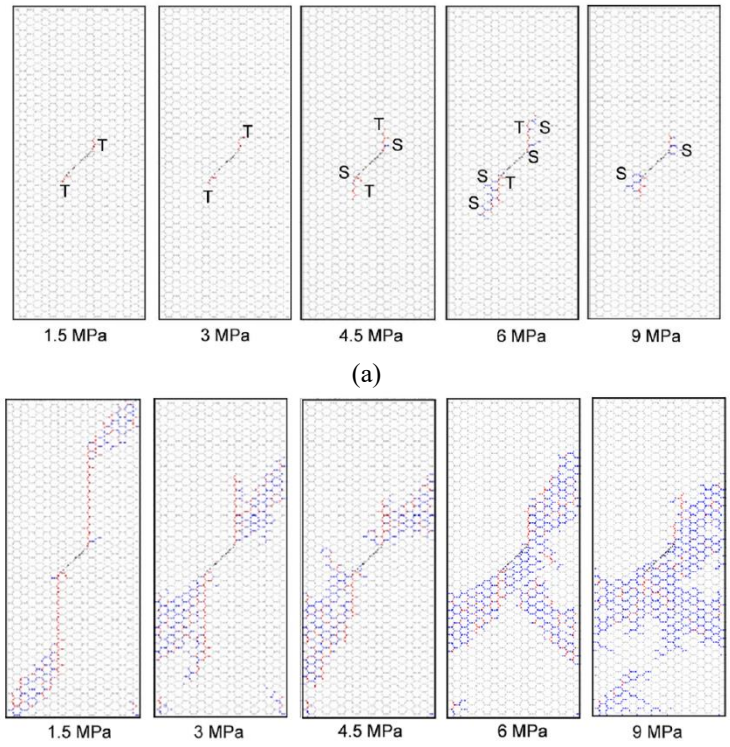

(a)

(b)

Fig. 42 (a) Formation of crack initiation is based on tensile, T (red colour contour) and shear, S (blue colour contour) nature and (b) Final failure of specimen under five different confinements (after Zhao *et al*. 2019)

of the wing crack was observed to be shorter than with 2.5 MPa confinement (Fig. 40(b)). At higher confinements, 7.5 MPa and 10 MPa, the wing cracks were not observed at the flaw's outer tip, and the coalescence was formed between quasi-coplanar secondary crack and secondary tensile crack (Fig. 40(c) and 40(d)). From the numerical study with an increase in confinement, the failure of the specimen changes from splitting failure to the shear failure mode. In addition to the effect of confinement, the nature coalescence was also observed to change due to an increase in the flaw number and continuity distance between the flaws based on study by Bi *et al.* (2016). They adopted General Particle Dynamics (GPD), a Meshless Numerical Method where analysis was carried out with four pre-existing flaws under single biaxial confinement, keeping the spacing constant and varying continuity (c) between the flaws 0, 1 and 2 times of flaw length. The formation of coalescence was observed by quasi-coplanar secondary cracks at the inner flaw tips and by oblique secondary cracks at the outer flaw tips for c=0 (Fig. 41(a)). When the continuity increases, the likely coalescence was observed from out-of-plane secondary crack and anti-wing crack between the inner flaw tips (Figs. 41(b) and 41(c)) and the specimen fails in shear mode under biaxial compression. The presence of macro-shear fractures was observed on the left and right sides of the specimen. A similar observation was also observed by

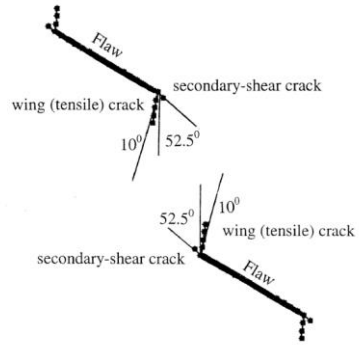

(a)

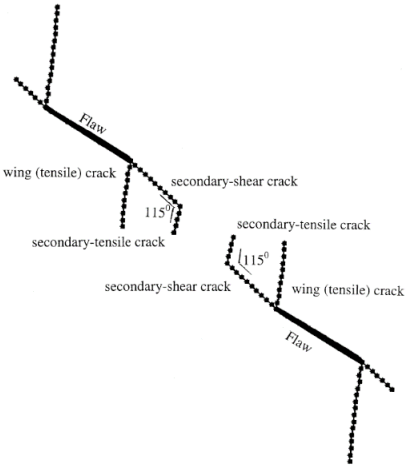

(b)

Fig. 43 (a) Initiation direction of tensile and shear cracks and (b) change in propagation direction obtained from numerical model (after Vásárhelyi and Bobet 2000)

Zhao *et al*. (2019) on single flaw specimens subjected to five different confinements (1.5, 3, 4.5, 6 and 9 MPa) using the expanded distinct element method (EDEM). From their analysis, like in previous studies, the tensile cracks were observed before shear cracks under low confining pressure (Fig. 42(a)). When the confinement level increases, both cracks initiate at the same stress level and the shear cracks are observed prior to tensile cracks at a higher level. This was due to confining pressure inhibiting the initiation of the tensile cracks. Further, from the aspect of specimen boundary, the lateral deformation gets limited due to the confining pressure which delays the tensile crack formation. Also, the crack propagation trajectories change their direction towards the horizontal direction, which causes the shear-based failure on the specimen at a higher confinement level (Fig. 42(b)).

3.2 Narrow flaw

Though many numerical studies were performed using different methods, the flaws were considered open and hence no interaction property was defined due to surface closure. Very limited studies were carried to consider the effect of friction resistance between the flawed surfaces due to closure. Based on the numerical study by Vásárhelyi and Bobet (2000) using FROCK, the direction of crack initiation for tensile and shear cracks was analysed for closed flaw configuration on a double flaw gypsum specimen adopted from Bobet and Einstein's (1998a) experimental study. From their analysis, the direction of the secondary crack increases to 52.5° and the wing crack initiates at about 62.5° with respect to the shear cracks (Fig. 43a), which is quite different from open flaws (Fig. 29(a)). They observed that the direction of both wing and shear cracks are independent of the flaw geometries. However, the crack initiation stress was influenced by flaw angle, spacing and continuity. A new secondary crack was observed as of a tensile nature, after the original secondary shear crack. The crack later propagates towards the direction of applied loading. Apart from these directions, they noticed that the length of the secondary crack lies in the range of 1.1-1.2 'a' (half of the flaw length) irrespective of open and closed flaw type. After it reaches the length, the crack propagation changes its orientation to about 115° and propagates as secondary tensile cracks (Fig. 43(b)). The effect of crack coalescence on frictional flaws (closed flaws) was observed to produce an additional coalescence mode by Tang *et al.* (2001) using RFPA code based on the finite element method. In their study, sandstone material with three flaws was adopted where one flaw was fixed at an angle of 45° and another flaw underneath whose angles are varied. Based on their results, under uniaxial compression, the coalescence apart from tensile (T) mode, shear mode (S), mixed tensile-shear mode (TS) and an additional compression mode (C) were observed (Fig. 44). The coalescence was observed forming by linkage of small-en echelon tensile crack that acts as a shear band. These small cracks are noticed under the local compressive stress field in the region where the shear band or fracture zone forms macroscopically. The analysis showed higher coalescence stress for shear mode than tensile and mixed-mode coalescences. It was concluded that the crack coalescence in three flaws occurs based on the weakest coalescence path between any two flaws. Further, the position of tensile crack was observed to change for both open and closed flaws from the numerical study by Sharafisafa and Nazem (2014) using the distinct element method, UDEC. From their model, the wing crack was often found to initiate from the flaw tips at a high flaw angle, and when the angle reduces, the crack initiation position shifts towards the flaw centre (Fig. 45). Also, no significant change was observed for crack coalescence behaviour for open and closed flaw configurations (Fig. 46).

Though, the tensile crack initiation stress for open flaw appears prior to closed flaw configuration, since the flaw surface in the latter has to overcome the surface friction to initiate the tensile crack. Later, the effect of surface friction between the flaw surfaces was studied by Xie *et al.* (2016) on a single flaw using the extended finite element method (XFEM). Their study investigated the effect of flaw surface friction on crack initiation and propagation for three different flaw angles (30˚, 45˚ and 60˚). The friction coefficients (μ) - 0, 0.1, 0.3 and 0.5 are adopted, where the adopted model could capture the variation in crack

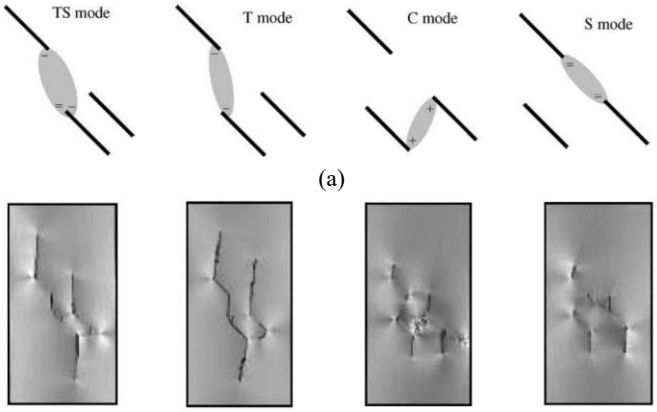

Fig. 44 Crack coalescence mode observed for three flaws based on (a) stress field interaction and coalescence path and (b) RFPA model (after Tang *et al*. 2001)

Fig. 45 Crack propagation was observed for same flaw geometry under (a) open and (b) closed flaws based on UDEC (after Sharafisafa and Nazem 2014)

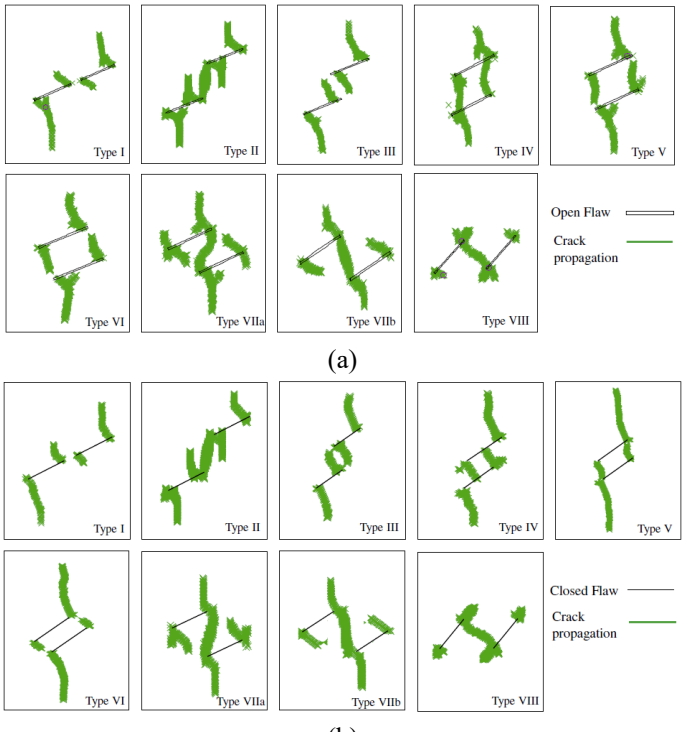

Fig. 46 Crack coalescence observed for (a) open and (b) closed flaw based on UDEC (after Sharafisafa and Nazem 2014)

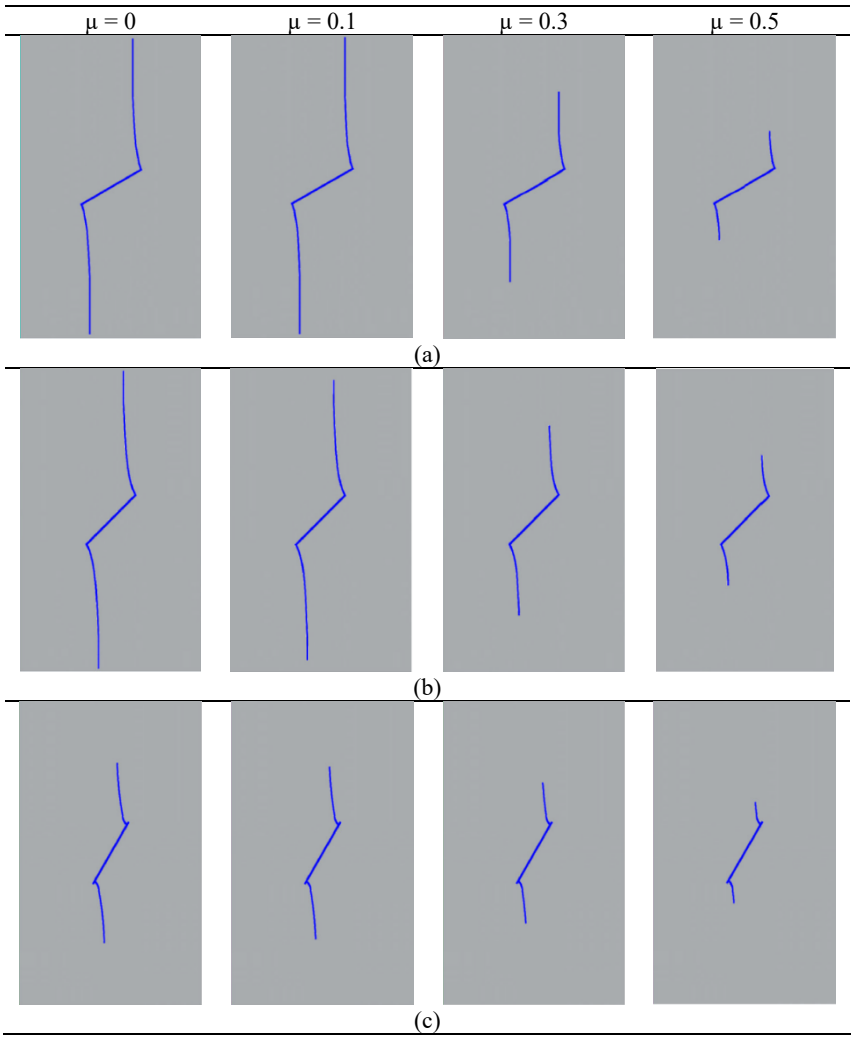

Fig. 47 Change in crack propagation by varying flaw surface friction (μ) for flaw angles (a) 30˚ (b) 45˚ and (c) 60˚ based on XFEM (after Xie *et al*. 2016)

propagation (Fig. 47). The analysis observed that the length of wing crack was longer for closed flaw conditions. But the wing crack length decreases with an increase in friction coefficient. Also, the surface friction across the flaw surface was found to increase with an increase in friction coefficient, and the flaw surface shear force decreases with an increase in flaw angle (Fig. 48). The shear force distribution at the flaw surface was observed at maximum at the centre of the surface and zero at the flaw tip. Apart from the change in friction coefficient, for the same surface friction, the shear force at the flaw surface for different flaw angles was systematically studied by Sivakumar and Maji (2021) on single and double flaws of non-parallel configuration using XFEM. The model adopts the cohesive zone model (CZM) to describe the onset and propagation of discontinuity (flaw) and using shear stress distribution, the possible formation of shear cracks was identified (Fig. 49).

The shear force distribution along the flaw length at the crack initiation was found to have a higher magnitude for low flaw angles from the single flaw configuration (Fig. 50(a)). Due to the effect of flaw closure between the surfaces observed in the experiments (Fig. 25(a)), a higher shear force was experienced. However, when the flaw angle increases, the surface closures become minimum and hence the shear force across the flaw length reduces. In the case of double flaw configuration, the shear force distribution on an inclined flaw was observed to be unsymmetrical compared to a single flaw (Fig. 50(b)). This was due to uneven stress distribution around the flaw tips where higher stress concentration at the left tip of the flaw was observed from the analysis (Fig. 49(b)). Nevertheless, the change in force distribution observed from double flaw are similar to the single flaw, where a higher magnitude of shear force was observed when the flaw is at a low angle.

Similar to the uniaxial compression study, Bobet and Einstein (1998b) observed an increase in crack stress levels for closed configurations compared to open flaw configurations under biaxial compression by using FROCK. The vertical stress was found to increase even after coalescence stress in the closed flaw type. Whereas in open flaw, where the vertical maximum stress was observed upto crack coalescence (Fig. 51). Under lower confinement levels, both tensile and shear cracks were observed to propagate further after reaching coalescence. With an

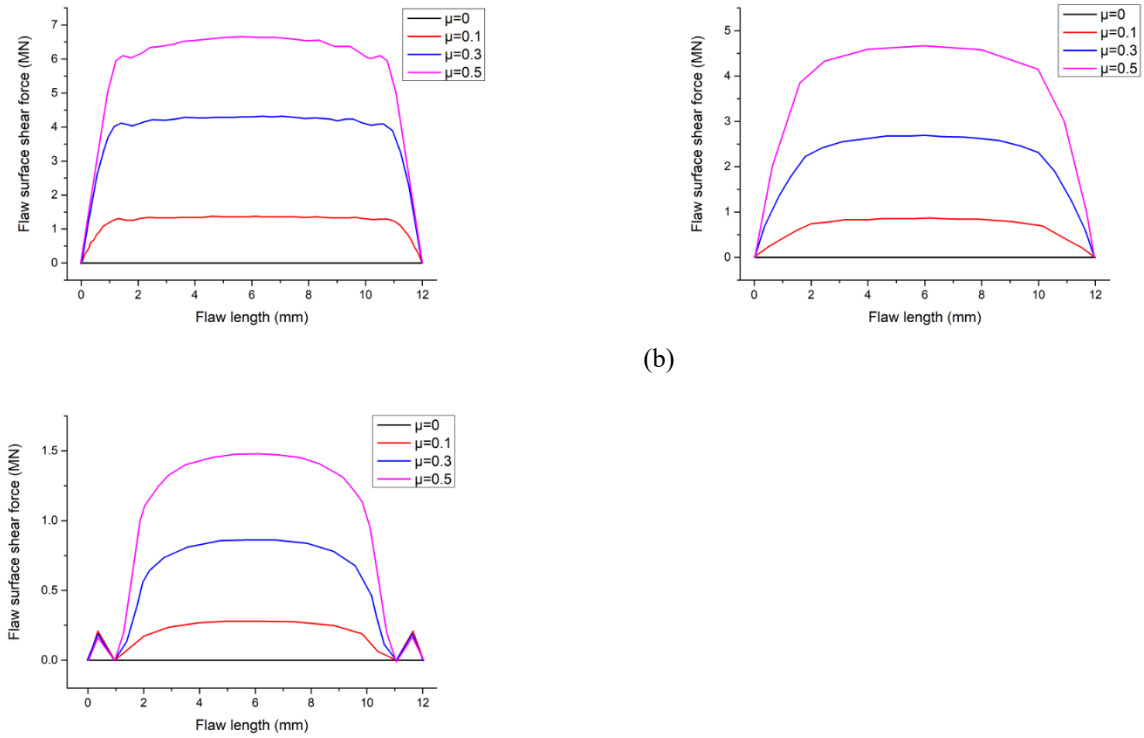

Fig. 48 Flaw surface shear force versus flaw length for angles (a) 30˚ (b) 45˚ and (c) 60˚ observed from XFEM (after Xie *et al.* 2016)

increase in confinement level, the tensile crack growth gets hampered, which causes the crack to grow smaller and more densely distributed with pre-existing flaws (Bobet and Einstein 1998a,b, Wang *et al.* 2014). Subsequently, due to localization, shear nature fractures are formed in the brittle material and later, after interaction between these fractures, a macro-failure was initiated in the rock specimen. The effect of crack growth with an increase in confinements for narrow flaw configuration was studied by Bi *et al.* (2016) using GPD on non-overlapping coplanar geometries. The wing cracks are first observed for uniaxial compression, initiating from both inner and outer tips, followed by quasi-coplanar direction shear crack and its subsequent coalescence (Fig. 52(a)). The material fails by the fully developed wing crack by splitting mode. When the lateral stress increases, the secondary cracks found to grow further, whereas the wing cracks get restrained. Under biaxial compression, the sample fails on the shear mode by splitting into fragments instead of a splitting failure observed from uniaxial compression (Fig. 52(b) and 52(c)). Also, the order of crack appearances changes, the wing crack was observed to be shifting towards the last appearance with an increase in confinement. For higher confinement, the crack appears only after coalescence between shear cracks and materials failed only by propagated quasi- shear crack under shear failure mode. Based on XFEM analysis by Haeri *et al.* (2020), similar to the previous studies (Xie *et al.* 2016, Sivakumar and Maji 2018, 2021), the crack stress behaviour of narrow flaw was found to be independent of the number of joints/flaws for varying flaw angles. The analysis was performed on flaw angles 0°, 45° and 90° with respect toloading directions for single, double and three flaws, and a flaw angle of 45° was observed favourable to crack to initiate first. The model showed that the tensile crack was usually the predominant fracturing mode observed under uniaxial compression. The tensile forces observed at the joint dip were higher than their shear strength. In narrow flaw angles, the initiation position of the tensile crack changes from the flaw tips for single and double joints to the mid-section of the flaw for three joints. The crack is always found to initiate at the tips for steep angles (Fig. 53). When the joint angle is 90º, the compressive strength becomes constant, however, Young's modulus decreases.

For other angles, the failure strength and Young's modulus decrease with an increase in joints and compressive strength was found to be minimum for 45º. Also, the tensile strength was found to decrease with an increase in joint angle and joint numbers. Recently, Wang and Wang (2022) adopted Discontinuous Deformation Analysis (DDA) method, which can simulate crack growth under both open and closed conditions. They adopted modified generalized tangential stress criteria and validated an experiment study by Miao *et al.* (2018) on red sandstone specimens with different infilling materials. The analysis was performed for four cases, with no filler, gypsum, cement and resin and compared their cracking behaviour with experiments (Fig. 54). For the filled flaw, the initiated tensile cracks from the flaw tips are suppressed and the

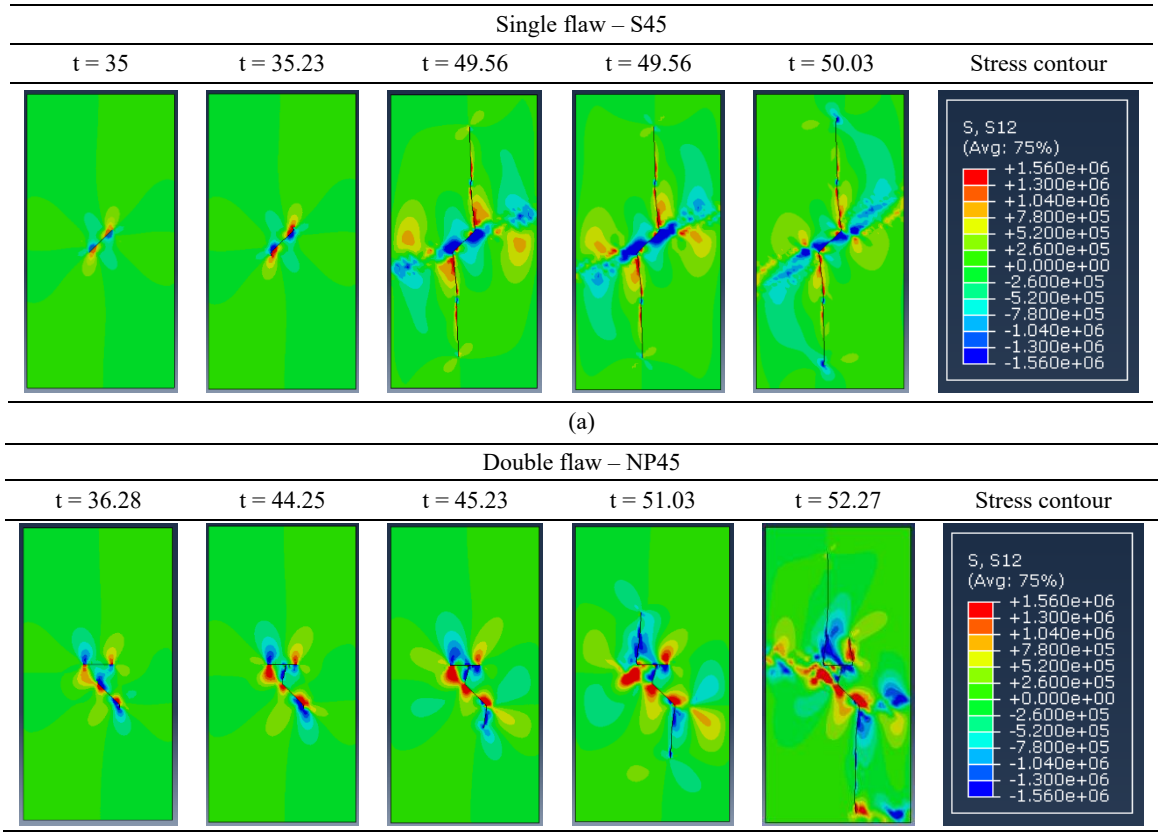

Fig. 49 Systematic behaviour of crack growth observed for (a) single flaw of angle 45º (S-45) and (b) non-parallel double flaw, where the inclined flaw of angle 45º (NP-45) based on shear stress distribution contour (after Sivakumar and Maji 2021)

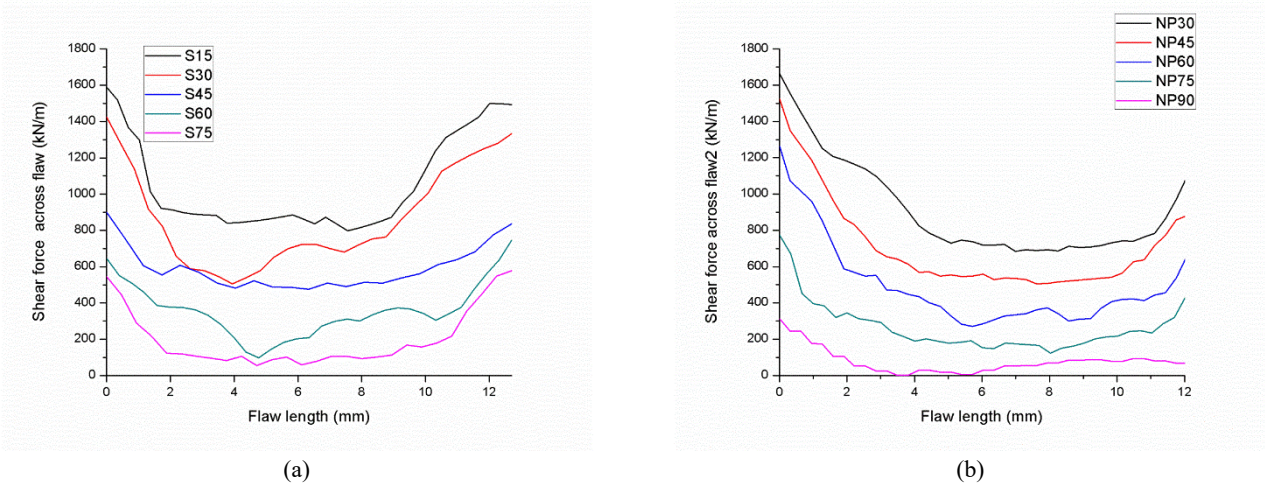

(a) (b)

Fig. 50 Shear force distribution observed for (a) single and double flaws along flaw length (after Sivakumar and Maji 2021)

propagated crack length found to be short and slim when compared the to unfilled flaw. Also, the specimen with a filled flaw showed higher crack initiation stress and a smaller crack initiation angle compared to the unfilled flaw. Previously, the DDA method was adopted by Wang *et al.* (2021) and used J-integral-based maximum circumferential tensile stress criteria. They simulated and validated the crack growth behaviour of a single flaw on cement mortar based on Jin *et al.* (2017) experiments. The model was analysed for three different flaw angles 30º, 60º and 75º subjected to uniaxial compression. However, they found that the model could simulate crack growth behaviour

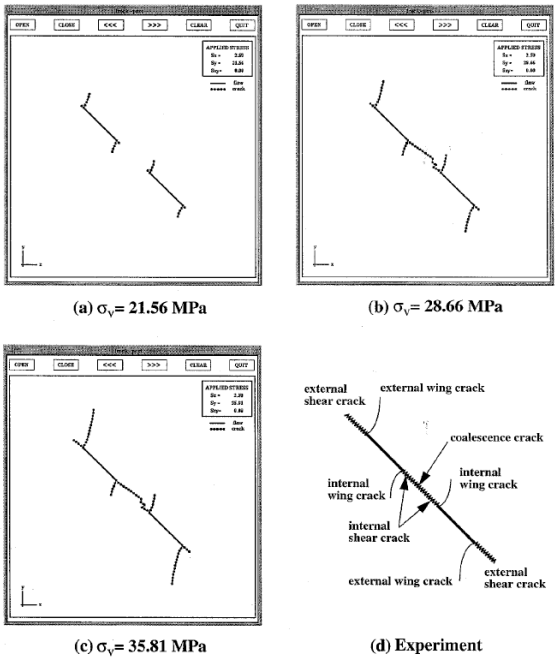

Fig. 51 Crack coalescence and propagation of cracks after their coalescence under biaxial compression for closed flaw geometry (after Bobet and Einstein 1998b)

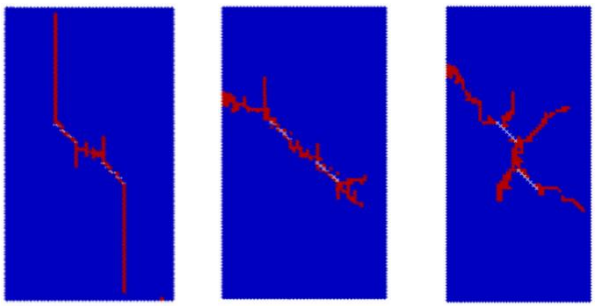

Fig. 52 Variation in crack coalescence under narrow flaw subjected to lateral confinements (a) 0 MPa, (b) 2.5 MPa and (c) 5 MPa (after Bi *et al.* 2016)

efficiently for higher flaw angles compared to low flaw angles (Fig. 55).

The literature discussed in the present study shows that the effect of friction between the flawed surfaces due to closure changes the cracking behaviour of the material.

From the systematic analysis of numerical models, narrow flaw configuration specimens often influence the initiation of crack and its propagation angle, which ultimately yields different failure patterns from open flaws. The change in crack propagation also leads to different coalescence behaviour even though the nature of cracks remains the same. By summarizing experiments and numerical studies, the crack stress behaviour is different from open flaw for different flaw angles and loading configurations. Also, very limited studies were performed on crack growth behaviour under biaxial compression and for non-parallel flaw configurations.

4. Conclusions

The failure modes observed in the rock under various stress conditions provide valuable information for safe and economical design in rocks. Their failure mechanism is strongly dependent on how the new cracks initiated and propagated from the fracture and their subsequent coalescence till forming a macro crack, and it will play a significant role in deciding the true strength of rocks. Apart from experimental studies, numerical methods on crack initiation and propagation have also significantly progressed in the last few decades. The present study mostly gives state-of-the-art in this area.

When subjected to external loading on rock, the mechanism of the non-persistent fractures leads to the development of a new crack and its propagation. Researchers have conducted experimental studies on crack growth in rock or rock-like materials subjected to different compressive loading environments. Those studies were also extended to numerical analysis with advancements in computational techniques. Literature shows that numerical modelling of crack growth can be systematically analyzed, especially of shear nature cracks where growth rates are highly unstable near the peak. Though many studies on non-persistent flaws for different geometrical arrangements, most of them are related to open flaw configurations. Limited literature found to have addressed narrow/closed flaws to understand the crack growth mechanism and their propagation pattern due to frictional resistance between the flaw surfaces.

Previous studies mostly categorized the crack initiation into many types, however most of them falls into two major crack nature types, tensile and shear. Previously they were interchangeably used as primary/wing cracks and secondary cracks respectively. For coalescence, modes are mainly tensile, shear or mixed tensile-shear observed in parallel flaws configurations. However, an additional compressive nature, or no coalescence mode observed for non-parallel configurations. Though overall cracking behaviour was quite similar, studies showed the change in crack initiation angle and order of appearance of predominant tensile and shear cracks could differentiate the cracking phenomenon between open and narrow/closed flaw configurations. The crack stresses are generally found to be higher for narrow flaw compared to open flaw configuration.

For a single flaw, on closed/narrow flaw conditions, the crack stress is generally found to decrease first, reach a minimum value generally at intermediate flaw angles (30º-60º) and later increase with increase in flaw angle. The behaviour is contradictory to the open flaw condition, where the flaw stress increases with increase in flaw angle. In case of double or multiple flaws, due to closure of flaw surface, the change in crack propagation path alters the crack coalescence behaviour and its failure mechanism. In case of biaxial compression, the difference between the open and narrow/closed flaw configuration remains the same however with increase in confinement their difference reduces. The above observations were commonly observed from experimental and numerical findings. However, the path of the crack propagation and its failure trajectory are well defined in the numerical model unlike the experiments. Also, the crack growth behaviour by numerical methods was found to be highly influenced by its method and

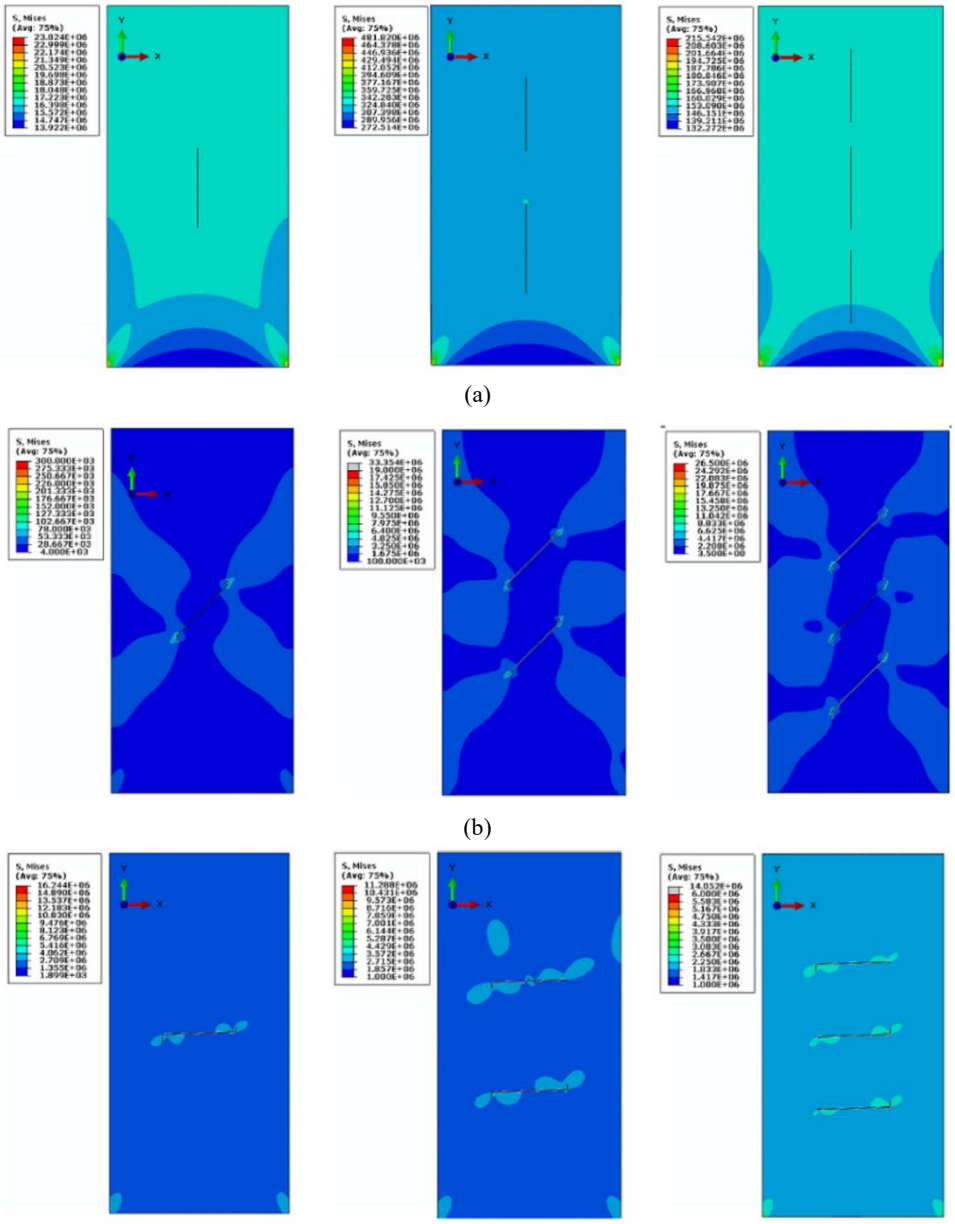

Fig. 53 Force distribution was observed on single, double and triple joints for flaw angles (a) 0°, (b) 45° and (c) 90° with respect to loading direction (after Haeri *et al*. 2020)

material criteria. This might not only alter the crack propagation path but also alters the change in crack stress level; hence a suitable criterion should be adopted based on field conditions.

The present review is limited to the crack growth behaviour of both configurations on open and closed/narrow flaws without any infilling material. The present paper discusses only considering the rock material as mostly isotropic and homogeneous, limiting to uniaxial and biaxial conditions. The effect of heterogeneity due to different mineral compositions or anisotropic effect could also alter the crack propagation path and its coalescence nature. Also, from the literature, it is understood that the rack growth and their coalescence behaviour studies on double flaws were mostly restricted within parallel and non-parallel configurations. Since the rock mass in the fields exhibits both random geometrical arrangements, which can also consist of both persistent and non-persistent fractures, the intersecting fractures should be considered for further studies.

References

Afolagboye, L.O., He, J. and Wang, S. (2018), "Crack initiation and coalescence behavior of two non-parallel flaws", *Geotech. Geol. Eng.*, **36**(1), 105-133. https://doi.org/10.1007/s10706-017-0310-0.

Amadei, B. and Goodman, R.E. (1981), "A 3-D Constitutive relation for fractured rock masses", *Proceedings of the International symposium on the Mechanical Behaviour of Structured Media*, Ottawa, 249-268.

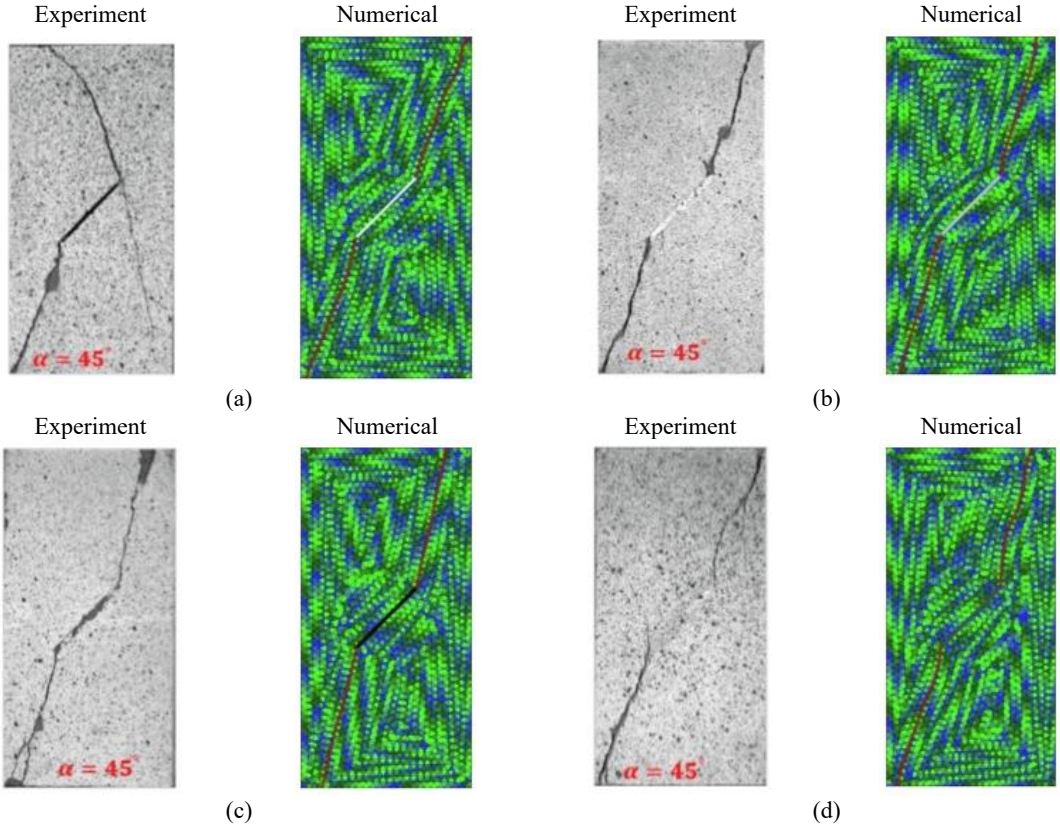

Fig. 54 Change in crack growth behavior observed for red sandstone with four infilling condition (a)no infill (b) gypsum (c) cement and (d) resin by comparing both experiment and numerical results (after Wang and Wang 2022)

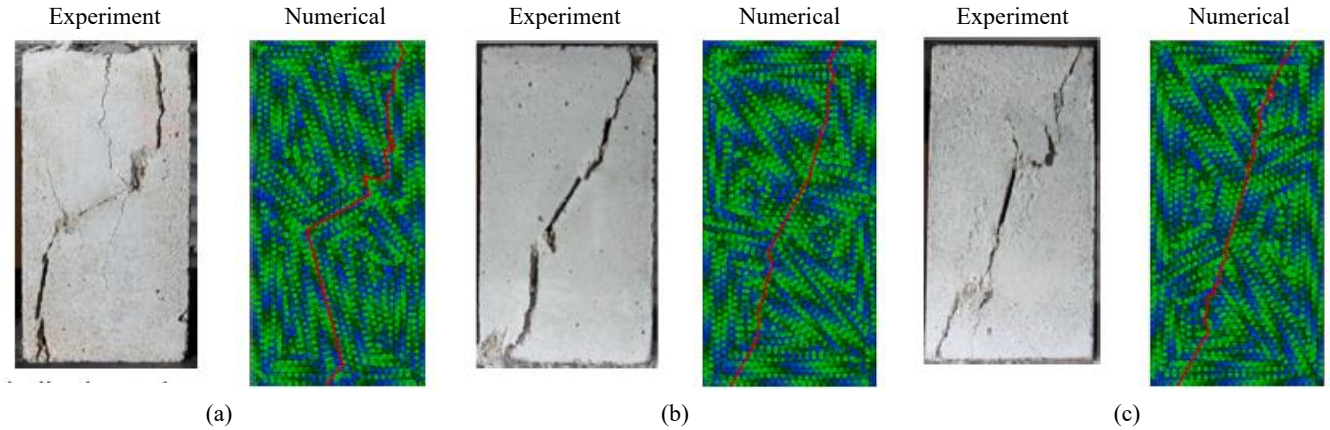

Fig. 55 Failure pattern observed from the experiment and numerical model using DDA single flaw angle at (a) 30˚ (b) 60˚ and (c) 75˚ by comparing both experiment and numerical results (after Wang *et al*. 2021)

Amini, M.S., Sarfarazi, V. and Babanouri, N. (2021), "Influence of non-persistent joint sets on the failure behaviour of concrete under uniaxial compression test", *Comput. Concrete*, **28**(3), 289-309. https://doi.org/10.12989/ cac.2021.28.3.289.

An, X., Ning, Y., Ma, G. and He, L. (2014), "Modeling progressive failures in rock slopes with non-persistent joints using the numerical manifold method", *Int. J. Numer. Anal. Method. Geomech.*, **38**, 679-701. https://doi.org/10.1002/nag.2226.

Ashby, M.F.A. and Hallam, S.D. (1986), "The failure of brittle solids containing small cracks under compressive stress states", *Acta Metallurgica,* **34**(3), 497-510. https://doi.org/10.1016/0001-6160(86)90086-6.

Bi, J., Zhou, X.P. and Qian, Q.H. (2016), "The 3D numerical simulation for the propagation process of multiple pre-existing flaws in rock-like materials subjected to biaxial compressive loads", *Rock Mech. Rock Eng.*, **49**(5), 1611-1627. https://doi.org/10.1007/s00603-015-0867-y.

Bobet, A. (1997), "Fracture coalescence in rock materials:

Experimental oberservations and Numerical Predictions", Sc.D, Thesis, Massachusetts Institute of Technology, Cambridge, MA.

Bobet, A. (2000), "The initiation of secondary cracks in compression", *Eng. Fract. Mech.*, **66**(2), 187-219. https://doi.org/10.1016/S0013-7944(00)00009-6.

Bobet, A. and Einstein, H.H. (1998a), "Fracture coalescence in rock-type materials under uniaxial and biaxial compression", *Int. J. Rock Mech. Min. Sci.*, **35**(7), 863-888. https://doi.org/10.1016/S0148-9062(98)00005-9.

Bobet, A. and Einstein, H.H. (1998b), "Numerical modeling of fracture coalescence in a model rock material", *Int. J. Fracture*, **92**, 221-252. https://doi.org/10.1023/A:1007460316400.

Brace, W.F. (1961), "Dependence of fracture strength of rocks on grain size", Bulletin of the Mimeral Industries Experiment Station Mining Engineering Series, Rock Mechanics, **76**, 99-103.

Chen, G., Kenmeny, M. and Harpalani, S. (1995), "Fracture propagation and coalescence in marble plates with pre-cut notches under compression", *Proceedings of the Symposium on fractured jointed rock masses*, Lake Tahoe, CA, USA.

Esterhuizen, G.S., Dolinar, D.R. and Ellenberger, J.L. (2011), "Pillar strength in underground stone mines in the United States", *Int. J. Rock Mech. Min. Sci*., 48(1), 42-50. https://doi.org/ 10.1016/J.IJRMMS.2010.06.003.

Goodman, R.E. (1989), *Introduction to Rock Mechanics*, Second Edition, Wiley Publication, New York, NY, USA.

Haeri, H., Sarfarazi, V., Ebneabbasi, P., Nazari-maram, A., Shahbazian, A., Marji, M.F. and Mohamadi, A.R. (2020), "XFEM and experimental simulation of failure mechanism of non-persistent joints in mortar under compression", *Constr. Build. Mater.*, **236**, 117500. https://doi.org/10.1016/j.conbuildmat.2019.117500.

Hoek, E. and Bieniawski, Z.T. (1965), "Brittle fracture propagation in rock under compression", *Int. J Fracture Mech.*, **1**(3), 139-155. https://doi.org/10.1007/BF00186851.

Hoek, E. and Bieniawski, Z.T. (1965), "Brittle fracture propagation in rock under compression", *Int. J. Fract. Mech.*, **1**(3), 139-155. https://doi.org/10.1007/BF00186851.

Hoek, E. and Martin, C.D. (2014), "Fracture initiation and propagation in intact rock – A review", *J. Rock Mech. Geotech. Eng.*, **6**, 287-300. https://doi.org/10.1016/j.jrmge.2014.06.001.

Huang, D., Gu, D., Yang, C., Huang, R. and Fu, G. (2015), "Investigation on mechanical behaviour of sandstone with two pre-existing flaws under triaxial compression", *Rock Mech. Rock Eng.*, **49**, 375-399. https://doi.org/10.1007/s00603-015-0757-3.

Huang, J., Chen, G., Zhao, Y. and Wang, R. (1990), "An experimental study of the strain field development prior to failure of a marble plate under compression", *Tectonophysics*, **175**, 269-284. https://doi.org/10.1016/0040-1951(90)90142-U.

Ingraffea, A.R. and Heuze, F.E. (1980), "Finite element models for rock fracture mechanics", *Int. J. Numer. Anal. Method. Geomech.*, **4**, 25-43. https://doi.org/10.1002/nag.1610040103.

ISRM (1978), "Suggested method for the quantitative description of discontinuities in rock masses", *Int. J. Rock Mech. Min. Sci. Geomech. Abstracts*, **15**, 319-368. https://doi.org/10.1016/0148-9062(78)91472-9.

Jade, S. and Sitharam, T.G. (2003), "Characterization of strength and deformation of jointed rock mass based on statistical analysis", *Int. J. Geomech.*, **3**(1), 43-54. https://doi.org/10.1061/(ASCE)1532-3641(2003)3:1(43).

Jaeger, J.C., Cook, N.G.W. and Zimmerman, R.W. (2007), *Fundamentals of Rock Mechanics*, Wiley-Blackwell Publication, UK.

Jin, J., Cao, P., Chen, Y., Pu, C., Mao, D. and Fan, X. (2017), "Influence of single flaw on the failure process and energy mechanics of rock-like material", *Comput. Geotech.*., **86**, 150-162. https://doi.org/10.1016/j.compgeo.2017.01.011.

Kang, G., Ning, Y., Chen, P., Pang, S. and Shao, Y. (2022), "Comprehensive simulations of rock fracturing with pre-existing cracks by the numerical manifold method", *Acta Geotechica*, **17**, 857-876. https://doi.org/10.1007/s11440-021-01252-3.

Lajtai, E.Z. (1974), "Brittle fracture in compression", *Int. J. Fracture*, **10**(4), 525-536. https://doi.org/10.1007/BF00155255.

Lee, H. and Jeon, S. (2011), "An experimental and numerical study of fracture coalescence in pre-cracked specimens under uniaxial compression", *Int. J. Solids Struct.*, **48**, 979-999. https://doi.org/10.1016/j.ijsolstr.2010.12.001.

Lee, J.L. and Hong, J.W. (2018), "Crack initiation and fragmentation processes in pre-cracked rock-like materials", *Geomech. Eng.,* **15**(5), 1047-1059. https://doi.org/10.12989/gae.2018.15.5.1047.

Li, H. and Wong, L.N.Y. (2012), "Influence of flaw inclination angle and loading condition on crack initiation and propagation", *Int. J. Solids Struct.*, **49**, 2482-2499. https://doi.org/10.1016/j.ijsolstr.2012.05.012.

Manoucherian, A. and Marji, M.F. (2012), "Numerical analysis of confinement effect on crack propagation mechanism from a flaw in a pre-cracked rock under compression", *Acta Mechanica Sinica*, **28**(5), 1389-1397. https://doi.org/10.1007/s10409-012-0145-0.

McClintock, F.A. and Walsh, J.B. (1962), "Friction on Griffith cracks in rocks under pressure", *Proceedings of the 4th US Congress Applied Mechanics*.

Miao, S., Pan, P-Z, Wu, Z., Li, S. and Zhao,S. (2018), "Fracture analysis of sandstone with a single filled flaw under uniaxial compression", *Eng. Fract. Mech.*, **204**, 319-343, https://doi.org/10.1016/j.engfracmech.2018.10.009.

Mughieda, O. and Karasneh, I. (2006), "Coalescence of offset rock joints under biaxial loading", *Geotech. Geol. Eng.*, **24**, 985-999. https://doi.org/10.1007/s10706-005-8352-0.

Park, C.H. and Bobet, A. (2009), "Crack coalescence in specimens with open and closed flaws: A comparison", *Int. J. Rock Mech. Min. Sci.*, **46**(5), 819-829. https://doi.org/10.1016/j.ijrmms.2009.02.006.

Park, C.H. and Bobet, A. (2010), "Crack initiation, propagation and coalescence from frictional flaws in uniaxial compression", *Eng. Fract. Mech.*, **77**(14), 2727-2748. https://doi.org/10.1016/j.engfracmech.2010.06.027.

Petit, J.P. and Barquins, M. (1988), "Can natural faults propagate under mode II conditions?", *Tectonics*, **7**(6), 1243-1256. https://doi.org/10.1029/TC007i006p01243.

Reyes, O. and Einstein, H.H. (1991), "Failure mechanism of fractured rock-a fracture coalescence model", *Proceedings of the 7th international congress on rock mechanics*, Germany.

Saberhosseini, S.E., Keshavarzi, R. and Ahangari, K. (2014), "A new geomechanical approach to investigate the role of in-situ stresses and pore pressure on hydraulic fracture pressure profile in vertical and horizontal oil wells", *Geomech. Eng.,* **7**(3), 233-246. https://doi.org/10.12989/gae.2014.7.3.233.

Sagong, M. and Bobet, A. (2002), "Coalescence of multiple flaws in a rock- model material in uniaxial compression", *Int. J. Rock Mech. Min. Sci.*, **39**(2), 229-241. https://doi.org/10.1016/S1365-1609(02)00027-8.

Sagong, M. and Bobet, A. (2002), "Coalescence of multiple flaws in a rock- model material in uniaxial compression", *Int. J. Rock Mech. Min. Sci.*, **39**(2), 229-241. https://doi.org/ 10.1016/S1365-1609(02)00027-8.

Sarfarazi, V., Abharian, S. and Ghalam E.Z. (2021), "Physical test and PFC2D simulation of the failure mechanism of echelon joint under uniaxial compression", *Comput. Concrete*, **27**(2), 99-109. https://doi.org/ 10.12989/cac.2021.27.2.099.

Sarfarazi, V., Wang, X., Nesari, M. and Ghalam, E.Z. (2022),

"Study of compressive behavior of triple joints using experimental test and numerical simulation", *Smart Struct. Syst.*, **30**(1), 49-62. https://doi.org/ 10.12989/sss.2022.30.1.049.

Sharafisafa, M. and Nazem, M. (2014), "Application of the distinct element method and the extended finite element in modelling cracks and coalescence in brittle materials", *Comput. Mater. Sci.*, **91**, 102-121. https://doi.org/10.1016/j.commatsci.2014.04.006.

Shemirani, A.B., Haeri, H., Sarfarazi, V. and Hedayat, A. (2017), "A review paper about experimental investigations on failure behaviour of non-persistent joint", *Geomech. Eng.*, **13**(4), 535-570. https://doi.org/10.12989/gae.2017.13.4.535.

Shen, B., Stephansson, O., Einstein, H.H. and Ghahreman, B. (1995), "Coalescence of fractures under shear stresses in experiments", *J. Geophys.Res.*, **100**(4), 5975-5990. https://doi.org/10.1029/95JB00040.

Sivakumar, G. and Maji, V.B. (2018), "A study on crack initiation and propagation in rock with pre-existing flaw under uniaxial compression", *Indian Geotech. J.*, **48**(4), 626-639. https://doi.org/10.1007/s40098-018-0304-8.

Sivakumar, G. and Maji, V.B. (2021), "Crack growth in rocks with pre-existing narrow flaws under uniaxial compression", *Int. J. Geomech.*, **21**(4), 04021032. https://doi.org/10.1061/(ASCE)GM.1943-5622.0001960.

Szwedzicki, T. (2007), "A hypothesis on modes of failure of rock samples tested in uniaxial compression", *Rock Mech. Rock Eng.*, **40**(1), 97-104. https://doi.org/10.1007/s00603-006-0096-5.

Tang, C.A., Lin, P., Wong, R.H.C. and Chau, K.T. (2001), "Analysis of crack coalescence in rock-like materials containing three flaws-Part II: numerical approach", *Int. J. Rock Mech. Min. Sci.*, **38**(7), 925-939. https://doi.org/10.1016/S1365-1609(01)00065-X.

Trivedi, A. (2013), "Estimating in situ deformation of rock masses using a hardening parameter and RQD", *Int. J. Geomech.*, **13**(4), 348-364. https://doi.org/10.1061/(ASCE)GM.1943-5622.0000215.

Vásárhelyi, B. and Bobet, A. (2000), "Modeling of crack initiation, propagation and coalescence in uniaxial compression", *Rock Mech. Rock Eng.*, **33**(2), 119-139. https://doi.org/10.1007/s006030050038.

Wang, C. and Wang, S. (2022), "Modified generalized maximum tangential stress criterion for simulation of crack propagation and its application in discontinuous deformation analysis", *Eng. Fract. Mech.*, **259**, 108159. https://doi.org/10.1016/j.engfracmech.2021.108159.

Wang, C., Wang, S., Chen, G., Yu, P. and Peng, X. (2021), "Implementation of a J-integral based maximum circumferential tensile stress theory in DDA for simulating crack propagation", *Eng. Fract. Mech.*, **246**, 107621. https://doi.org/10.1016/j.engfracmech.2021.107621

Wang, T.T. and Huang, T.H. (2009), "A constitutive model for the deformation of a rock mass containing sets of ubiquitous joints", *Int. J. Rock Mech. Min. Sci.*, **46**(3), 521-530. https://doi.org/10.1016/j.ijrmms.2008.09.011.

Wang, Y., Zhou, X. and Xu, X. (2016), "Numerical simulation of propagation and coalescence of flaws in rock materials under compressive loads using the extended non-ordinary state-based peridynamics", *Eng. Fract. Mech.*, **163**, 248-273. https://doi.org/10.1016/j.engfracmech.2016.06.013.

Wawersik, W.R. and Fairhurst, C. (1970), "A study of brittle rock fracture in laboratory compression experiments", *Int. J. Rock Mech. Min. Sci. Geomech. Abstracts*, **7**(5), 561-575. https://doi.org/10.1016/0148-9062(70)90007-0.

Wong, L.N.Y. and Einstein, H.H. (2009a), "Systematic evaluation of cracking behavior in specimens containing single flaws under uniaxial compression", *Int. J. Rock Mech. Min. Sci.*, **46**(2), 239-249. https://doi.org/10.1016/j.ijrmms.2008.03.006.

Wong, L.N.Y. and Einstein, H.H. (2009b), "Crack coalescence in molded gypsum and Carrara marble: Part 1-macroscopic observations and interpretation", *Rock Mech. Rock Eng.*, **42**(3), 475-511. https://doi.org/10.1007/s00603-008-0002-4.

Wong, L.N.Y. and Einstein, H.H. (2009c), "Crack coalescence in molded gypsum and Carrara marble: Part 2-microscopic observations and interpretation" *Rock Mech. Rock Eng.*, **42**(3), 513-545. https://doi.org/10.1007/s00603-008-0003-3.

Wong, R.H. and Chau, K.T. (1998), "Crack coalescence in a rock-like material containing two cracks", *Int. J. Rock Mech. Min. Sci.*, **35**(2), 147-164. https://doi.org/10.1016/S0148-9062(97)00303-3.

Wong, R.H.C., Guo, Y.S.H., Li, L.Y., Chau, K.T., Zhu, W.S. and Li, S.C. (2006), "Anti-wing crack growth from surface flaw in real rock under uniaxial compression", *Proceedings of the 16th European Conference on Fracture (EFC16)*, Alexandroupolis, Greece.

Wu, Z. and Wong, L.N.Y. (2012), "Frictional crack initiation and propagation analysis using the numerical manifold method", *Comput. Geotech.*, **39**, 38-53. https://doi.org/ 10.1016/j.compgeo.2011.08.011.

Xie, Y., Cao, P., Liu, J. and Dong, L. (2016), "Influence of crack surface friction on crack initiation and propagation: A numerical investigation based on extended finite element method", *Comput. Geotech.*, **74**, 1-14. https://doi.org/10.1016/j.compgeo.2015.12.013.

Yang, S.Q. and Jing, H.W. (2011), "Strength and crack coalescence behavior of brittle sandstone samples containing a single fissure under uniaxial compression", *Int. J. Fracture*, **168**, 227-250. https://doi.org/10.1007/s10704-010-9576-4.

Yang, S.Q., Jiang, Y.Z., Xu, W.Y. and Chen, X.Q. (2008), "Experimental investigation on strength and failure behaviour of pre-cracked marble under conventional triaxial compression", *Int. J. Solids Struct.*, **45**(15), 4796-4819. https://doi.org/10.1016/j.ijsolstr.2008.04.023

Yang, SQ (2015), "An experimental study on fracture coalescence characteristics of brittle sandstone specimens combined various flaws", *Geomech. Eng.*, **8**(4), 541-557. https://doi.org/10.12989/gae.2015.8.4.541.

Zhang, X.P. and Wong, L.N.Y. (2012), "Cracking process in rock-like material containing a single flaw under uniaxial compression: a numerical study on parallel bonded-particle model approach", *Rock Mech. Rock Eng.*, **45**, 711-737. https://doi.org/10.1007/s00603-011-0176-z.

Zhang, X.P. and Wong, L.N.Y. (2013), "Crack initiation, propagation and coalescence in rock-like material containing two flaws: a numerical study based on bonded-particle model approach", *Rock Mech. Rock Eng.*, **46**(5), 1001-1021. https://doi.org/10.1007/s00603-012-0323-1.

Zhang, X.P., Liu, Q., Wu, S. and Tang, X. (2015), "Crack coalescence between two non-parallel flaws in rock-like material under uniaxial compression", *Eng. Geol.*, **199**, 74-90. https://doi.org/10.1016/j.enggeo.2015.10.007.

Zhao, C., Zhou, Y., Zhang, Q., Zhao, C. and Matsuda, H. (2019), "Influence of inclination angles and confining pressures on mechanical behavior of rock materials containing a pre-existing crack", *Int. J. Numer. Analytical Method. Geomech.*, **44**, 353-370. https://doi.org/10.1002/nag.3003.

Zhao, Y., Zhang, L., Wang, W., Pu, C., Wan, W. and Tang, J. (2016), "Cracking and stress-strain behaviour of rock-like material containing two flaws under uniaxial compression", *Rock Mech. Rock Eng.*, **49**(7), 2665-2687. https://doi.org/10.1007/s00603-016-0932-1.

CC